NASA TECHNICAL NOTE

NASA TN D-2602

NASA TN D-2602

c. 1

FLIGHT-MEASURED WING SURFACE PRESSURES AND LOADS FOR THE X-15 AIRPLANE AT MACH NUMBERS FROM 1.2 TO 6.0

by Jon S. Pyle

Flight Research Center
Edwards, Calif.

NATIONAL AERONAUTICS AND SPACE ADMINISTRATION • WASHINGTON, D. C. • JANUARY 1965

FLIGHT-MEASURED WING SURFACE PRESSURES AND LOADS FOR THE X-15 AIRPLANE AT MACH NUMBERS FROM 1.2 TO 6.0

By Jon S. Pyle

Flight Research Center
Edwards, Calif.

NATIONAL AERONAUTICS AND SPACE ADMINISTRATION

For sale by the Office of Technical Services, Department of Commerce,
Washington, D.C. 20230 -- Price $2.00

FLIGHT-MEASURED WING SURFACE PRESSURES AND LOADS FOR THE X-15 AIRPLANE AT MACH NUMBERS FROM 1.2 TO 6.0

By Jon S. Pyle
Flight Research Center

SUMMARY

Flight-measured pressure distributions are presented for the upper and lower surfaces on the wing and wing-body juncture of the X-15 airplane at angles of attack from 0° to 20° and Mach numbers from 1.2 to 6.0. Aerodynamic loads derived from surface pressure measurements are presented as spanwise load distributions and total exposed wing-panel loads.

The results of the investigation indicate that chordwise and spanwise centers of pressure remain fairly constant as Mach number increases. Isolated-wing theories (shock expansion and linear) generally underestimated the aerodynamic loads, with the exception of pitching moment. Linear theory (wing in presence of body) gave fair predictions of the experimental lift-curve slopes at the lower angles of attack.

The agreement between flight measurements and wind-tunnel results was well within the accuracy of the data.

INTRODUCTION

The X-15 research airplane was designed for flight investigations at supersonic and hypersonic speeds. The structural design required consideration of both thermal and aerodynamic loads under highly transient flight conditions. Therefore, surface pressure orifices were installed at various locations on the airplane to aid in the analysis of aerodynamic heating and to obtain aerodynamic loads.

Preliminary chordwise and spanwise load distributions on the X-15 wing panel were reported in reference 1 at angles of attack of 10° and 15° and Mach numbers of 4.7 and 5.4. Wing-panel lift-curve-slope data were obtained from surface pressure orifices and strain gages at angles of attack between 0° and 5°. Although the lift-curve slopes obtained from the strain gages compare favorably with those from pressure distributions, the thermal effects on the strain gages resulted in unreliable values of absolute loads for temperatures above about 500° F. Thus, at present, it is believed that absolute values of flight-measured aerodynamic loads and load distributions for the X-15 under quasi-steady-state

conditions can be obtained more reliably from surface pressure distributions than from strain gages.

This paper presents flight-measured surface pressure distributions for the wing and wing-body juncture and the associated derived aerodynamic loads for angles of attack from 0° to 20° and Mach numbers from 1.2 to 6.0. These data are compared with data from wind-tunnel tests conducted in 1960 (ref. 2) and with predicted values from shock-expansion and linear theories (refs. 3 to 5).

SYMBOLS

$b/2$ wing semispan, measured from fuselage centerline to wing tip, ft

$b'/2$ wing-panel semispan, measured from wing station 44 (wing side-fairing junction, fig. 3) to wing tip, ft

C_B wing-panel bending-moment coefficient about wing station 44 (fig. 3), $\int_0^1 c_n \frac{c}{c_{av}} \frac{y'}{b'/2} \, d\frac{y'}{b'/2}$

C_m wing-panel pitching-moment coefficient about $0.25\bar{c}$, $\frac{c_{av}}{\bar{c}} \int_0^1 c_m \left(\frac{c}{c_{av}}\right)^2 d\left(\frac{y'}{b'/2}\right)$

C_N wing-panel normal-force coefficient, $\int_0^1 c_n \frac{c}{c_{av}} \, d\left(\frac{y'}{b'/2}\right)$

$C_{N_\alpha} = \frac{dC_N}{d\alpha}$

C_p pressure coefficient, $\frac{p_d + p_r - p_\infty}{q}$

C_{p_l} pressure coefficient on lower wing surface

c local wing chord, streamwise, ft

$\bar{c}$ mean aerodynamic chord of wing panel, $\frac{1}{S'} \int_0^{b'/2} c^2 dy'$, ft

c_{av} average chord of wing panel parallel to plane of symmetry, $\frac{S'}{b'/2}$, ft

c_m section pitching-moment coefficient about 0.25c,

$$\int_0^1 \frac{p_l - p_u}{q}\left(0.25 - \frac{x}{c}\right)d\left(\frac{x}{c}\right)$$

c_n section normal-force coefficient parallel to plane of symmetry,

$$\int_0^1 \frac{p_l - p_u}{q}\, d\left(\frac{x}{c}\right)$$

M free-stream Mach number

p local static pressure, lb/sq ft absolute

p_d differential pressure, $p - p_r$, lb/sq ft

p_l local static pressure on lower wing surface, lb/sq ft absolute

p_u local static pressure on upper wing surface, lb/sq ft absolute

p_r reference pressure, lb/sq ft absolute

p_∞ free-stream static pressure, lb/sq ft absolute

q free-stream dynamic pressure, lb/sq ft absolute

S' area of wing panels outboard of wing station 44 (fig. 3), sq ft

X_{cp} wing-panel chordwise center of pressure, $0.25 - \frac{C_m}{C_N}$, percent $\bar{c}$

x distance rearward of leading edge of local chord parallel to plane of symmetry, ft

Y_{cp} wing-panel spanwise center of pressure, $\frac{C_B}{C_N}$, percent $b'/2$

y spanwise distance outboard of fuselage centerline, ft

y' spanwise distance outboard of wing station 44 (fig. 3), ft

α airplane angle of attack, deg

Δ root-mean-square error

DESCRIPTION OF AIRPLANE AND MODEL

The X-15 (figs. 1 and 2) is a rocket-powered research airplane designed to attain hypersonic speeds and altitudes in excess of 250,000 feet. A detailed description of the airplane and the control systems is presented in reference 6.

The exposed wing panel has a modified NACA 66005 airfoil section with a taper ratio of 0.27 and an aspect ratio of 2.15. The leading edge is swept back 36.75°, and the trailing edge is swept forward 17.74°. The wing flaps, located next to the side fairing at the trailing edge of the wing, are deflected downward 32° and are used for landing purposes only. Other pertinent dimensions and physical characteristics of the wing are presented in table I.

The 0.0667-scale model of the X-15 used in the Langley Research Center wind-tunnel tests differed slightly from the actual airplane in wing profile ahead of the 15-percent chord. The local airfoil section tangent slopes at their respective percent chords for the root (wing station 44) and tip are as follows:

Wing chord, percent	Wing tangent coordinates			
	Model		Flight	
	Root	Tip	Root	Tip
0	0	0	0	0
1.25	0.490	0.833	0.287	0.837
2.50	.318	.450	.213	.449
5	.213	.252	.170	.252
7.50	.171	.184	.151	.185
10	.146	.151	.138	.152
15	.117	.117	.117	.117
20	.100	.100	.100	.100

INSTRUMENTATION AND ACCURACY

Airplane

The surface pressure orifices on the X-15 airplane (fig. 3) consist of 1/4-inch inner-diameter titanium tubing mounted flush with the external surface of the skin. Each orifice is connected to standard NASA 24-cell mechanical-optical manometers by 1/4-inch inner-diameter aluminum tubing and rubber connectors. Tubing lengths ranged from 15 feet to 30 feet. Data were obtained under quasi-steady-state flight conditions. The time lag in the system was considered to be negligible, on the basis of the studies of reference 7.

Surface pressures were measured with differential-pressure cells having a root-mean-square error of ±10 lb/sq ft. The reference pressure (instrument compartment) was measured with absolute-pressure cells having a root-mean-square error of ±6.5 lb/sq ft. These errors were combined by taking the square root of the sum of their squares to give the estimated root-mean-square error in the measured surface pressures. The following estimated errors in other quantities pertinent to this investigation were obtained from reference 8:

Δp_∞, lb/sq ft	$\pm 0.04 p_\infty$
ΔM	±0.07
$\Delta\alpha$, deg	±0.75

The standard deviation in the pressure coefficient ΔC_p was determined as follows

$$\Delta C_p = \left[\left(\frac{\partial C_p}{\partial p_d}\right)^2 \Delta p_d{}^2 + \left(\frac{\partial C_p}{\partial p_r}\right)^2 \Delta p_r{}^2 + \left(\frac{\partial C_p}{\partial p_\infty}\right)^2 \Delta p_\infty{}^2 + \left(\frac{\partial C_p}{\partial M}\right) \Delta M^2\right]^{1/2} \tag{1}$$

Differentiating $C_p = \dfrac{p_d + p_r - p_\infty}{q}$ and substituting gives

$$\Delta C_p = \left\{\left(\frac{1}{q}\right)^2 \left[\Delta p_d{}^2 + \Delta p_r{}^2 + \left(\frac{p_d + p_r}{p_\infty}\right)^2 \Delta p_\infty{}^2 + \frac{4}{M^2}\left(p_d + p_r - p_\infty\right)^2 \Delta M^2\right]\right\}^{1/2} \tag{2}$$

The standard deviation of pressure coefficient, calculated by using equation (2), varies between ±0.04 at an angle of attack of 10° (M = 2.3) and ±0.03 at an angle of attack of 15° (M = 4.7). The values of ΔC_p from equation (2) decrease with increasing Mach number and dynamic pressure. Since the pressure coefficient is indirectly a function of angle of attack (C_p increases with increasing angle of attack, as shown in the flight-data analysis), the values of ΔC_p decrease with decreasing angles of attack.

Model

The maximum probable error in the wind-tunnel pressure coefficients reported in reference 2 varied from ±0.018 at M = 2.3 to ±0.033 at M = 4.65. The maximum deviation in Mach number was ±0.02 at M = 2.3 and M = 2.8 and ±0.05 at M = 4.65. Angle-of-attack and angle-of-sideslip errors were not presented.

TESTS

Airplane

Data were obtained up to an altitude of 100,000 feet ($p_\infty > 20$ lb/sq ft). The data presented herein were chosen from time intervals in which the dynamic pressure was equal to or greater than 500 lb/sq ft, with the exception of Mach numbers below 2.3 for which available data were limited. In this region, therefore, some data are presented at dynamic pressures less than 500 lb/sq ft. Angles of attack presented are nominal values and are within ±0.75° of the value shown. To minimize sideslip effects, the flight data were selected from flight conditions for which the angles of sideslip were less than ±1°.

Because of the airplane trim limits, data within the Mach number range from 1.8 to 3.0 at angles of attack greater than 10° are not available. Also, data are not presented below a Mach number of 1.2 because of the large measurement errors at the lower dynamic pressures.

Model

The 0.0667-scale model wind-tunnel tests were conducted in the Langley Unitary Plan wind tunnel. Mach numbers were varied from 2.30 to 4.65 by means of an asymmetrical sliding-block nozzle, which permits a continuous variation of Mach number.

The test conditions for the flight measurements and wind-tunnel results presented herein were as follows:

Wind tunnel		Flight	
M	α, deg	M	α, deg
----	----------	1.2	5, 10
----	----------	1.4	5, 10, 15
----	----------	1.8	0, 5, 10
2.30	0, 5, 10	2.3	0, 5, 10
2.88	0, 5, 10	3.0	0, 5, 10
----	----------	4.0	0, 5, 10, 15, 20
4.65	0, 5, 10, 15	4.7	0, 5, 10, 15
----	----------	5.0	0, 5, 10, 20
----	----------	5.5	0, 5, 10, 15
----	----------	6.0	0, 5

PRESENTATION OF RESULTS

X-15 flight-measured wing surface pressures are presented as chordwise pressure distributions in figures 4(a) to 4(j). Shown are upper and lower surfaces of root, midsemispan, and tip orifice rows of the wing for Mach numbers from 1.2 to 6.0 and angles of attack from 0° to 20°. Where applicable, the data are compared to wind-tunnel results and shock-expansion theory (ref. 3).

Figure 4(i) (α = 10°, midsemispan) shows a higher pressure coefficient than was reported in reference 1. (For example, the pressure coefficient measured at the 0.27 chord is 0.20, compared to 0.15 in reference 1.) This increase is based on data obtained from several flights after the publication of reference 1; whereas, the data reported at a Mach number of 5.4 in reference 1 were from only one flight on which, it was later determined, some instruments were inaccurate.

Three chordwise measurements on the midsemispan orifice row are shown with increasing Mach number in figure 5 as a summary of the pressure-distribution data of figure 4. The locations of the bow and side-fairing shocks (reproduced from unpublished wind tunnel Schlieren photographs) are presented in figure 6 to show the effects of the shocks on the chordwise pressure distributions. The shock profiles are shown for three Mach numbers and for angles of attack of 0° and 10°.

Pressure coefficients are presented in figures 7(a) to 7(d) to show the spanwise pressure distributions over the wing, side fairing, and fuselage. The orifices used to measure these pressure distributions are shown along the dashed line in figure 3.

Spanwise load distributions derived from the area enclosed by the upper and lower surface pressure distributions of figure 4 are presented in figures 8(a) to 8(j). Distributions for the full-scale flight vehicle, a scaled wind-tunnel model, and shock-expansion (isolated wing) theory are compared. Linear theories (isolated wing and wing in presence of body, refs. 4 and 5, respectively) are also shown to compare linearity and body effect with the loads distributions.

Figures 9(a) to 9(j) present the resultant loads on the X-15 wing panel for increasing angles of attack and for Mach numbers from 1.2 to 6.0. Flight data are compared with wind-tunnel results and theoretical predictions.

The resultant loads of figure 9 are compared with the preliminary strain-gage data of reference 1 in figure 10, a summary of chordwise and spanwise center-of-pressure data and lift-curve slopes with increasing Mach number. The strain-gage data represent slopes at angles of attack from 0° to 5°; whereas, the flight data and theoretical predictions are for an angle of attack of 10°.

DISCUSSION OF RESULTS

A general reduction of pressure coefficient with increasing Mach number is shown in the chordwise pressure distributions of figure 4. The noticeable

reductions of pressure coefficient on the tip chord (figs. 4(a) to 4(c)) are caused by a local expansion of the flow around the tip.

Reasonably good agreement between shock-expansion theory and experimental results (flight pressure measurements and wind-tunnel results) is evident at the lower Mach numbers of 1.8, 2.3, 3.0, and 4.0 (figs. 4(c), 4(d), 4(e), and 4(f), respectively). However, as the bow and side-fairing shocks move near the mid-semispan orifice row of the wing (fig. 6(b)), the flow over the wing is compressed (shown as an increase in pressure coefficient). These flow compressions are shown in figure 5 at Mach numbers above 4.0. The shock-expansion theory (using free-stream conditions) does not adequately predict the increase in pressure coefficients, as indicated by the comparison with experimental results in figures 4(g) to 4(j).

At angles of attack of 5° and 10° (fig. 8), the agreement of theoretical predictions with experimental results is fairly good. However, at the higher angles of attack (figs. 8(f) to 8(i)), the linear theories do not predict the increased loading shown by the flight data. Although the shock-expansion theory does not adequately predict the distribution of the spanwise loads, it approximates the resultant loads on the wing, as shown in figure 9.

The resultant loads on the wing (fig. 9) indicate the trends of the experimental data as angle of attack increases. Comparison of theoretical and experimental results shows that the theory predicts the general trends of the data, with the following exceptions: The shock-expansion theory predicts the nonlinearity of the lift-curve slopes at the higher angles of attack but underestimates the loads at the lower angles of attack, except for pitching moments, which are overestimated in a negative direction. Linear (isolated wing) theory does not predict the nonlinearity of the lift-curve slopes and generally underestimates the loads; however, with the wing in the presence of the body, reasonable estimates of the low angle-of-attack loads were obtained.

The chordwise and spanwise centers of pressure (fig. 10) remained fairly constant on the wing panel over the Mach number range investigated. Although theoretical predictions of the locations of spanwise and chordwise centers of pressure were fairly accurate, the theories indicated that the spanwise center of pressure was farther outboard than shown by the flight values and that the chordwise center of pressure was farther rearward of the leading edge than indicated by the flight data.

The flight strain-gage lift-curve slopes of reference 1 are slightly lower than the experimental results presented in figure 10. The theoretical predictions indicate the general reduction of lift-curve slope with Mach number; however, the comparison again shows a general underestimation of the results.

Although some differences are noted between pressure distributions obtained from flight data and from wind-tunnel tests, generally good agreement within the accuracy of the measurements is indicated throughout the investigation.

SUMMARY OF RESULTS

Surface pressure measurements over the wing of the X-15 airplane at Mach numbers from 1.2 to 6.0 and at angles of attack from 0° to 20° indicate the following:

1. Chordwise and spanwise centers of pressure remained fairly constant as Mach number increased.

2. With the exception of pitching-moment coefficient, isolated-wing theories generally underestimated the aerodynamic loads. Linear theory (wing in presence of body) compared favorably with the measured data at the lower angles of attack but underestimated the wing lift-curve slopes at the higher angles of attack. Shock-expansion (isolated wing) theory agreed more closely with measured loads over the high angle-of-attack range of the tests.

3. The agreement between flight measurements and wind-tunnel results was well within the accuracy of the measurements.

Flight Research Center,
National Aeronautics and Space Administration,
Edwards, Calif., October 27, 1964.

REFERENCES

1. Keener, Earl R., and Pembo, Chris: Aerodynamic Forces on Components of the X-15 Airplane. NASA TM X-712, 1962.

2. Hodge, B. Leon, and Burbank, Paige B.: Pressure Distribution of a 0.0667-Scale Model of the X-15 Airplane for an Angle-of-Attack Range of 0° to 28° at Mach Numbers of 2.30, 2.88 and 4.65. NASA TM X-275, 1960.

3. Ames Research Staff: Equations, Tables, and Charts for Compressible Flow. NACA Rep. 1135, 1953.

4. Martin, John C., and Jeffreys, Isabella: Span Load Distributions Resulting From Angle of Attack, Rolling, and Pitching for Tapered Sweptback Wings With Streamwise Tips - Supersonic Leading and Trailing Edges. NACA TN 2643, 1952.

5. Pitts, William C., Nielsen, Jack N., and Kaattari, George E.: Lift and Center of Pressure of Wing-Body-Tail Combinations at Subsonic, Transonic, and Supersonic Speeds. NACA Rep. 1307, 1957.

6. Finch, Thomas W., and Matranga, Gene J.: Launch, Low-Speed, and Landing Characteristics Determined From the First Flight of the North American X-15 Research Airplane. NASA TM X-195, 1959.

7. Saltzman, Edwin J.: Base Pressure Coefficients Obtained From the X-15 Airplane for Mach Numbers Up to 6. NASA TN D-2420, 1964.

8. Larson, Terry J., and Webb, Lannie D.: Calibrations and Comparisons of Pressure-Type Airspeed-Altitude Systems of the X-15 Airplane From Subsonic to High Supersonic Speeds. NASA TN D-1724, 1963.

TABLE I.- DIMENSIONS AND CHARACTERISTICS OF THE EXPOSED X-15 WING PANEL

Airfoil section	NACA 66005 (modified)
Total area, sq ft	105.02
Span, ft	14.96
Aspect ratio	2.15
Taper ratio	0.27
Mean aerodynamic chord, ft	7.76
Chord, ft	
Root	11
Tip	2.98
Sweepback, deg	
Leading edge	36.75
0.25 chord	25.64
Trailing edge	-17.74
Dihedral, deg	0
Incidence, deg	0
Aerodynamic twist, deg	0
Flap	
Area (each), ft	8.30
Span (each), ft	4.50
Ratio of flap chord to wing chord	0.22
Ratio of total flap area to total wing area	0.08
Chord, ft	
Inboard	2.61
Outboard	1.08
Deflection down, deg	
Original	40
Present	32
Sweepback angle of hinge line, deg	0
Trailing-edge sweep angle, deg	-17.74

E-7903

Figure 1.- X-15 airplane.

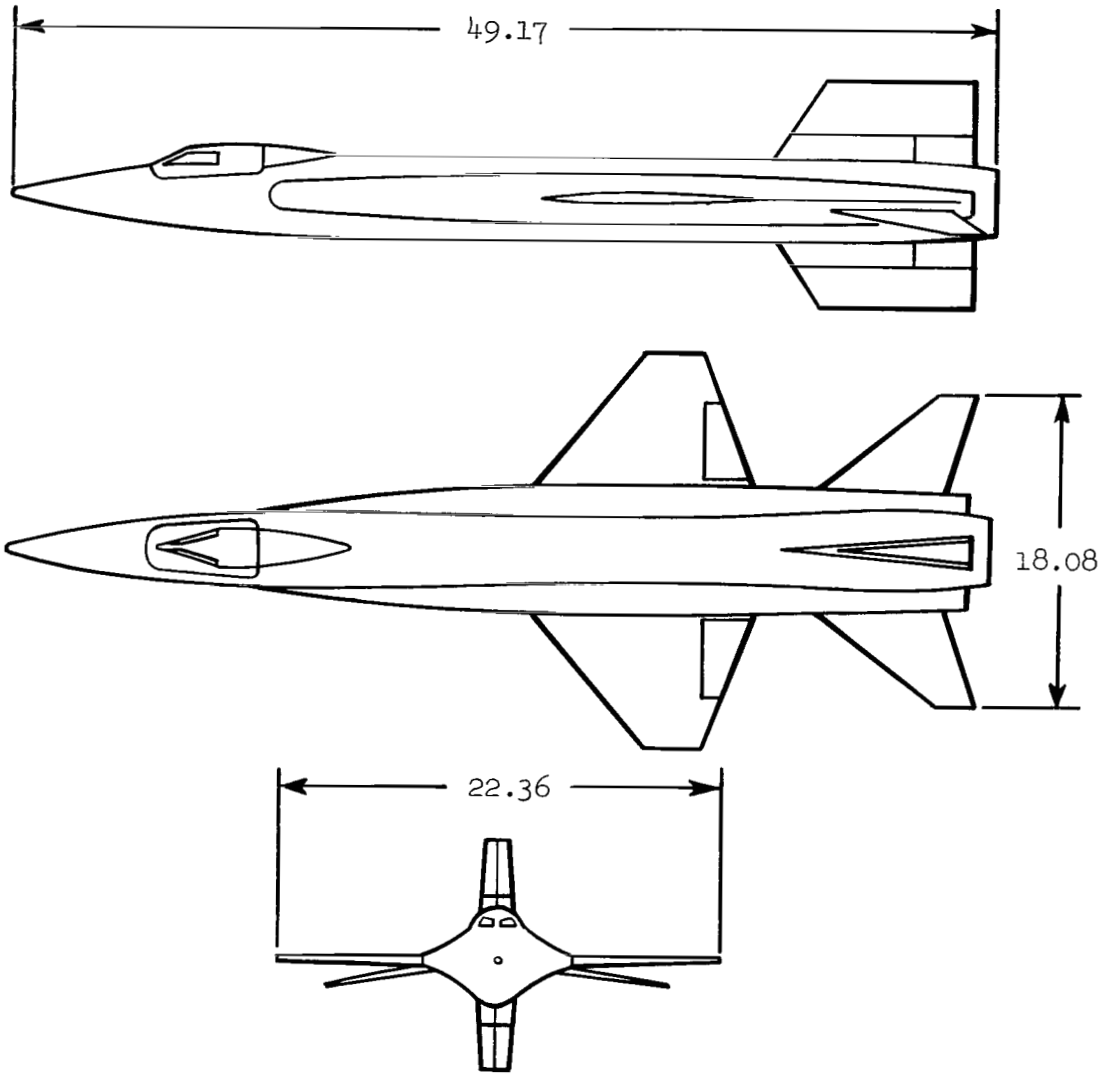

Figure 2.- Three-view drawing of X-15 airplane. Dimensions in feet.

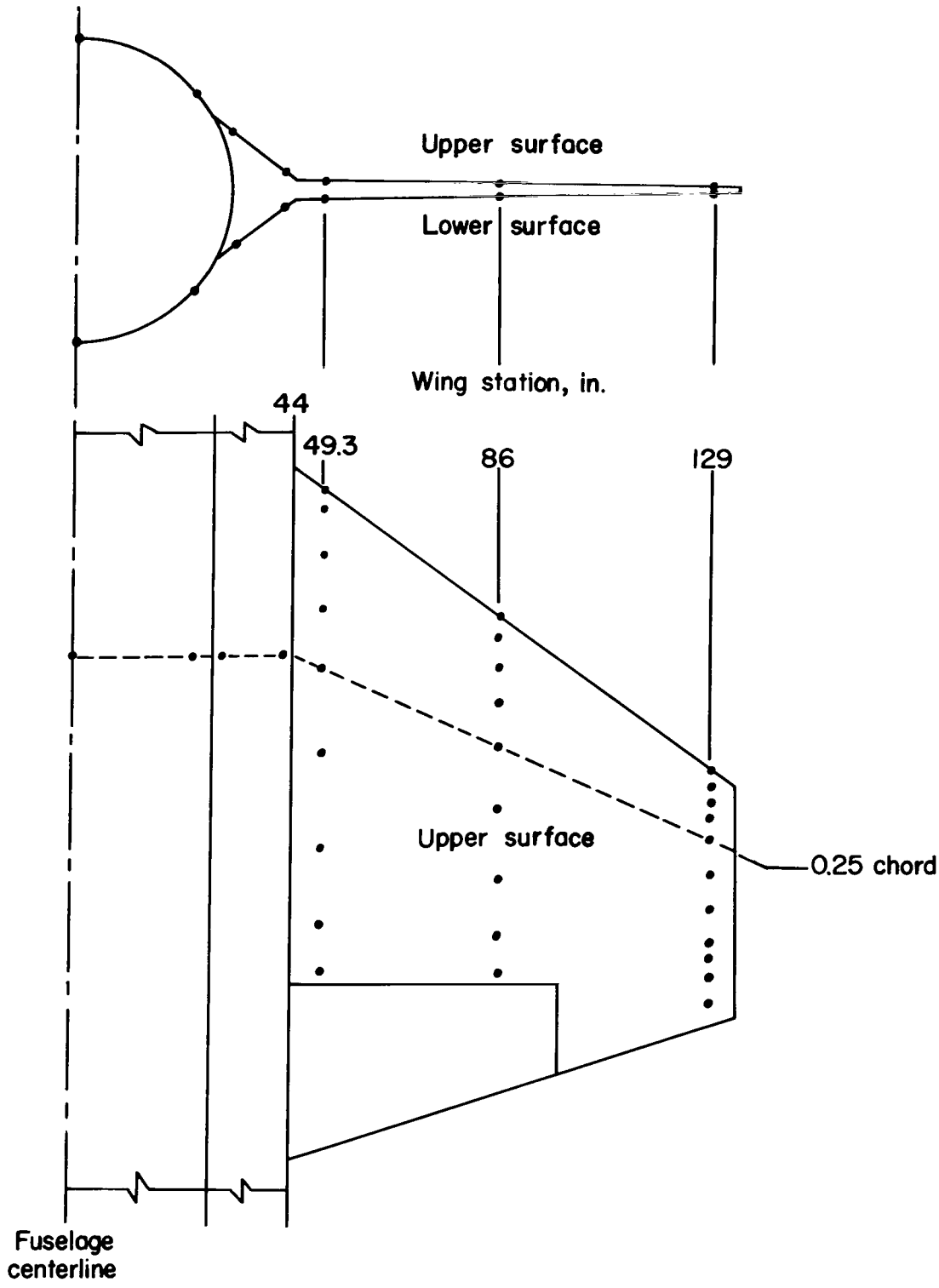

Figure 3.- Pressure orifices on the fuselage and wing of the X-15.

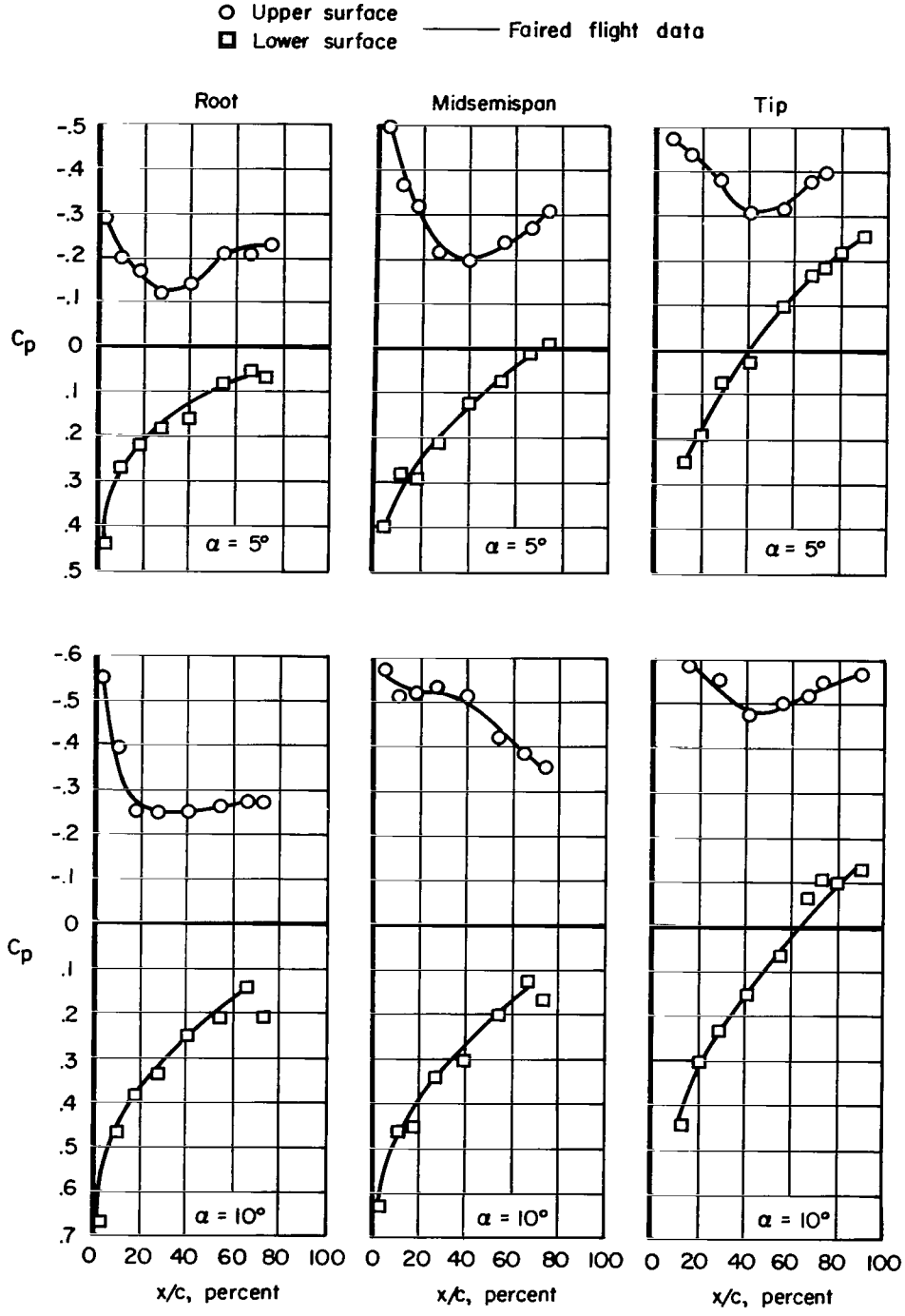

(a) M = 1.2.

Figure 4.- Chordwise pressure distributions on the X-15 wing.

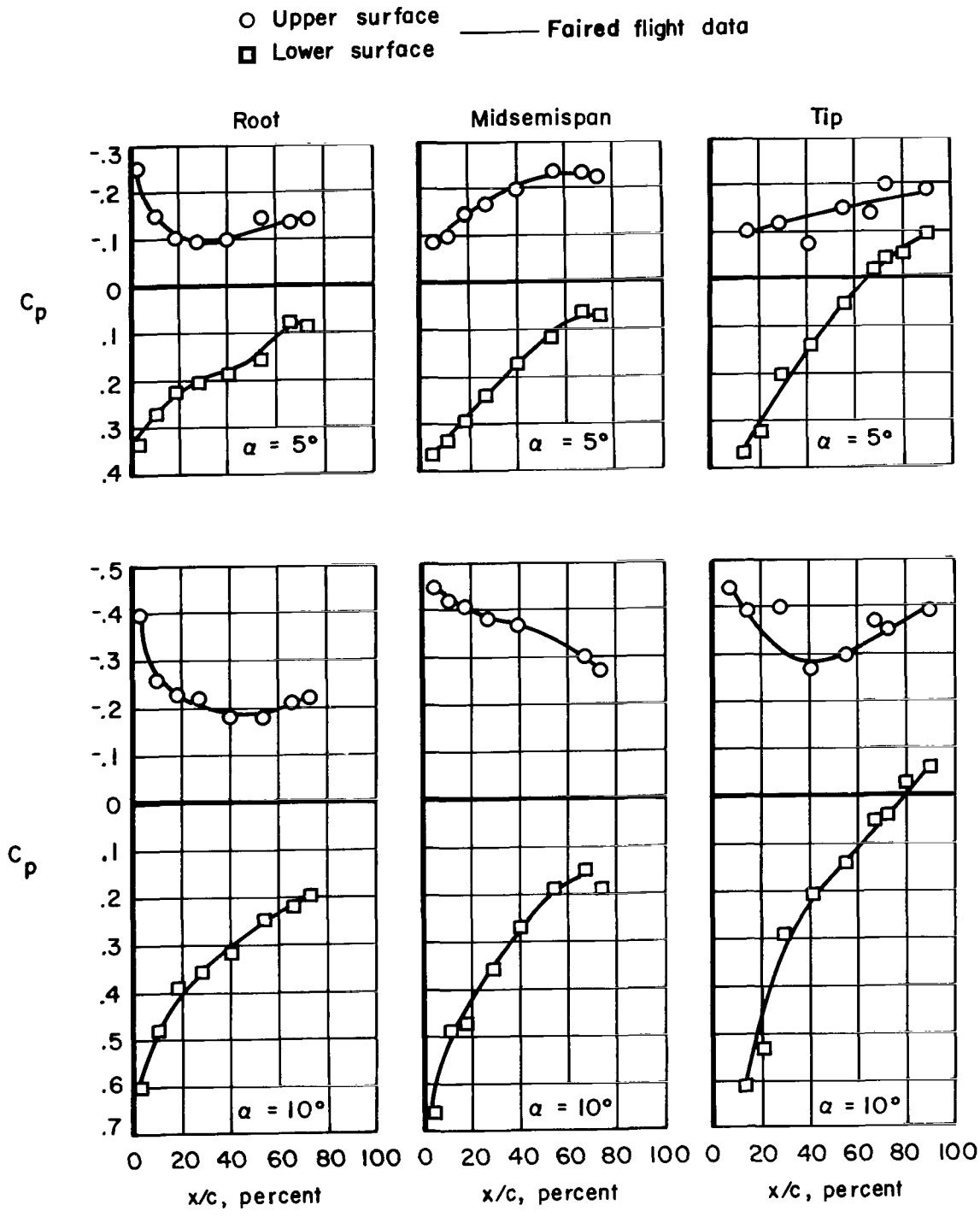

(b) M = 1.4.

Figure 4.- Continued.

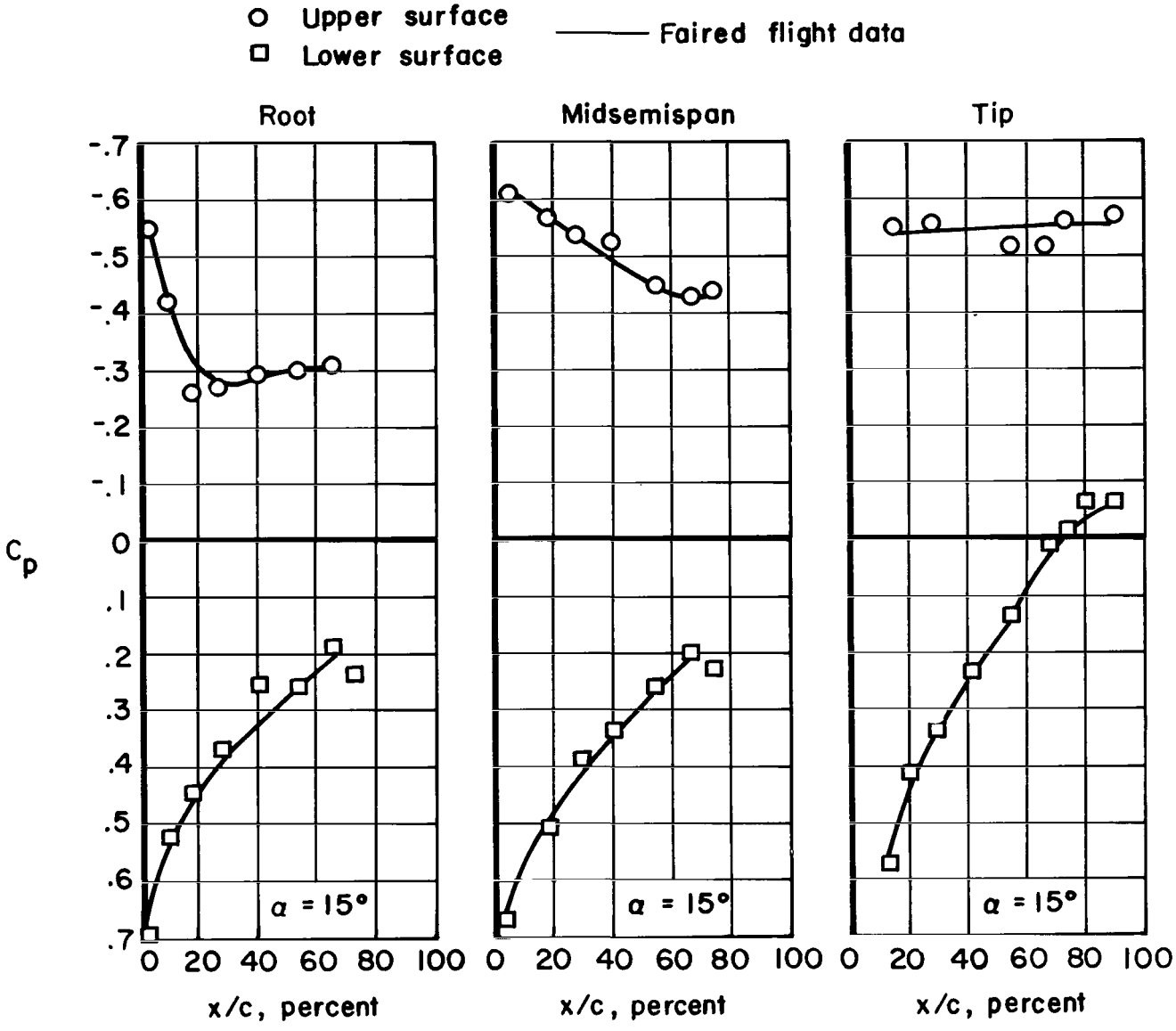

(b) M = 1.4 (concluded).

Figure 4.- Continued.

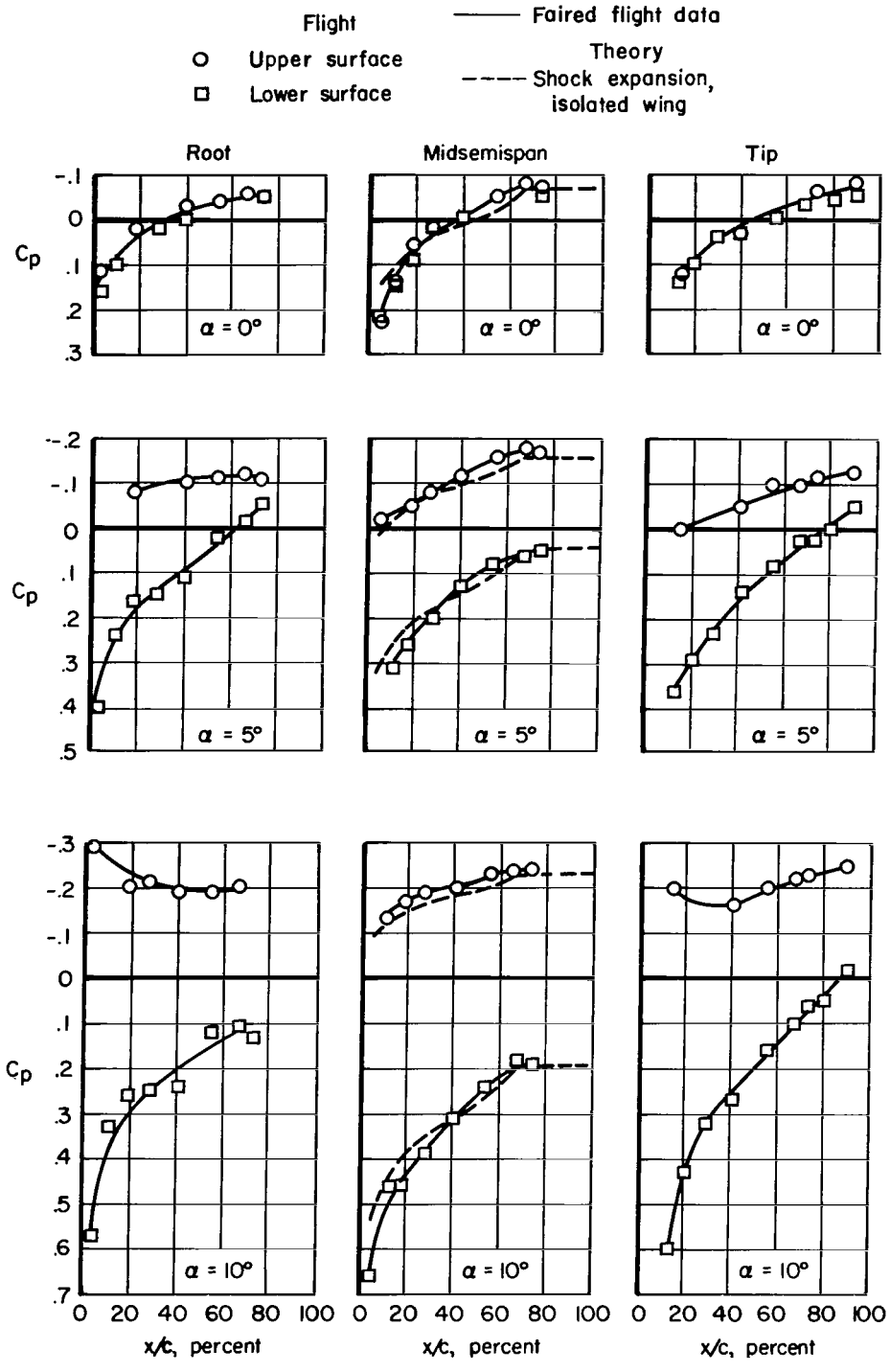

(c) M = 1.8.

Figure 4.- Continued.

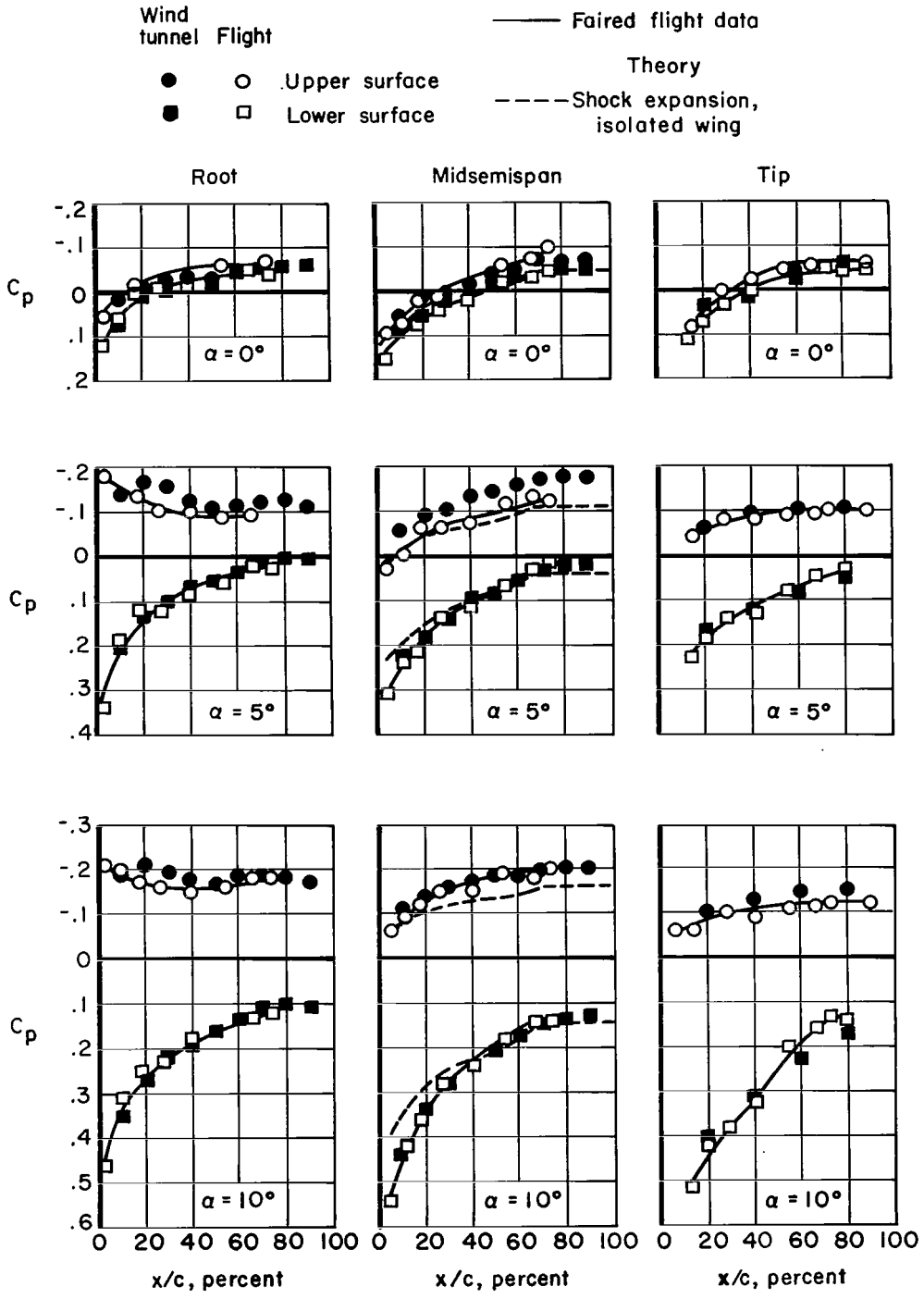

(d) M = 2.3.

Figure 4.- Continued.

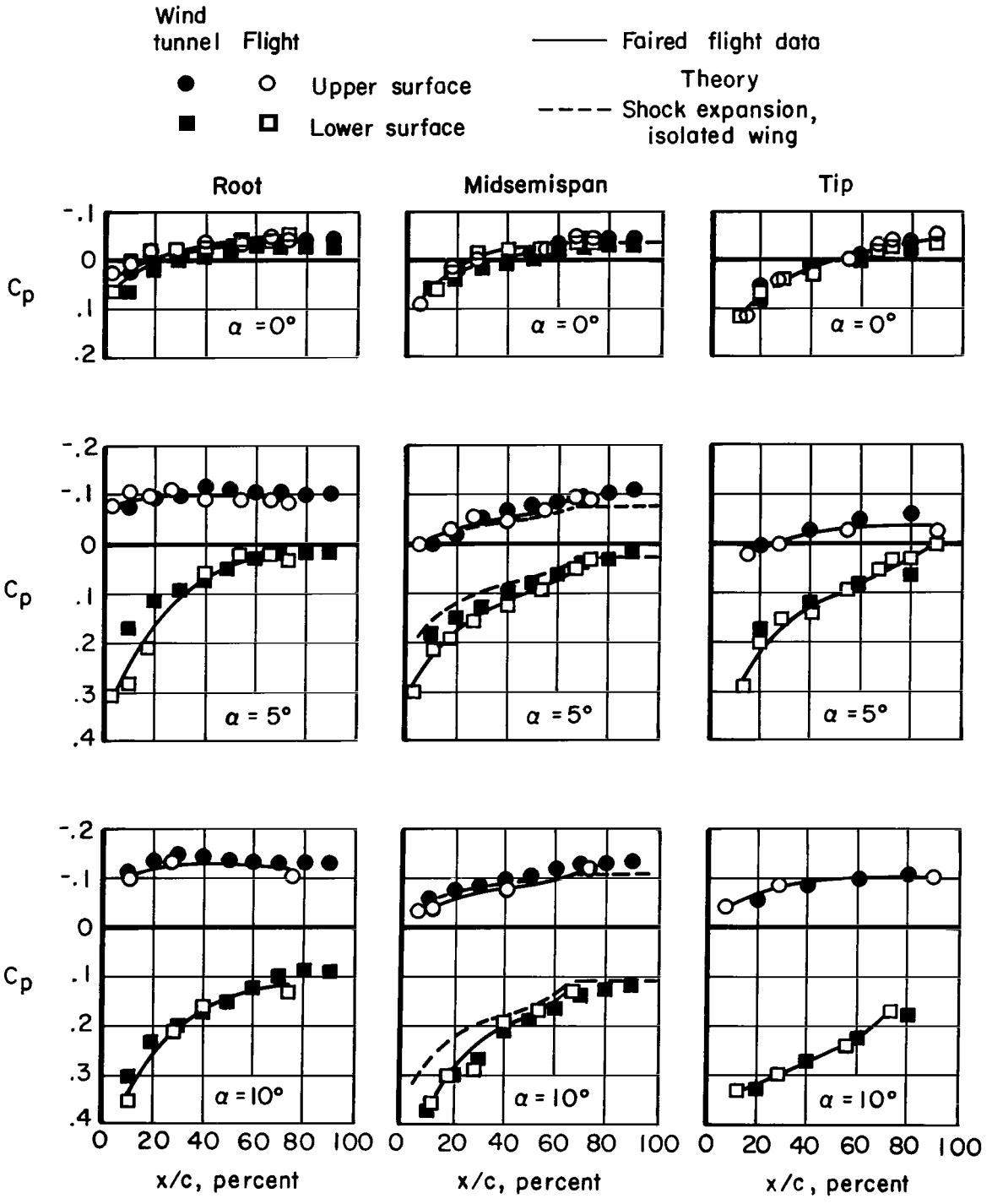

(e) M = 3.0.

Figure 4.- Continued.

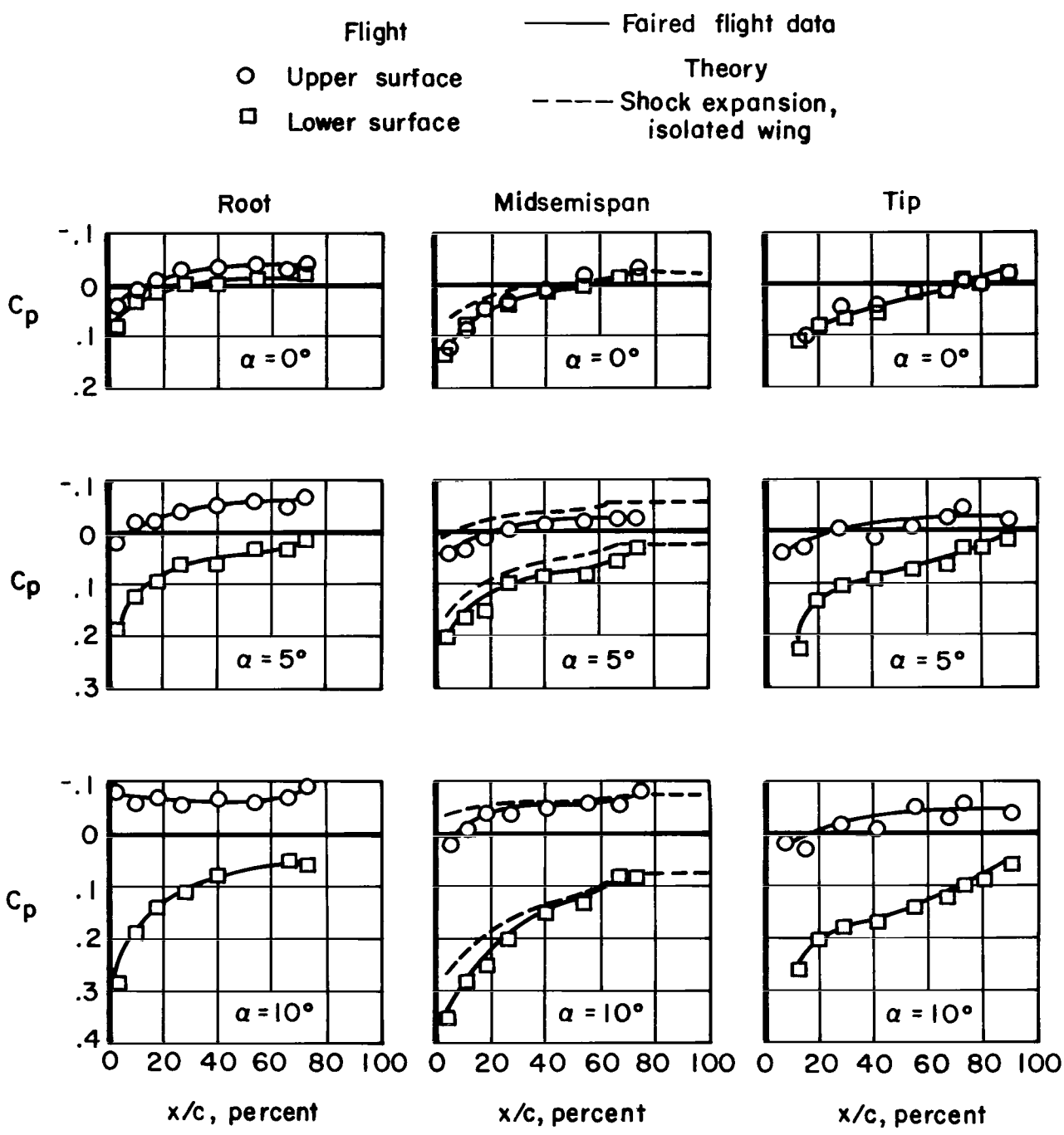

(f) M = 4.0.

Figure 4.- Continued.

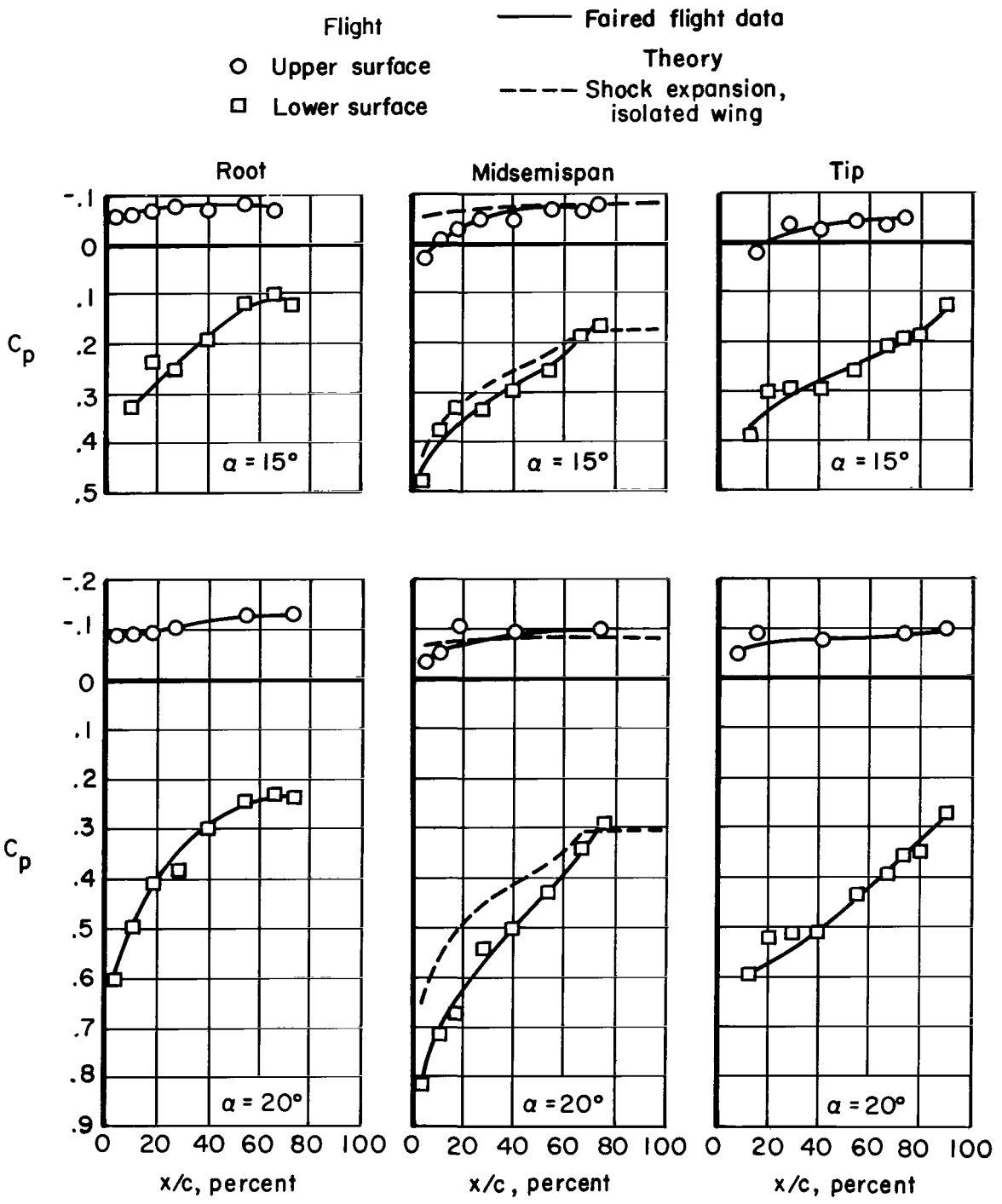

(f) M = 4.0 (concluded).

Figure 4.- Continued.

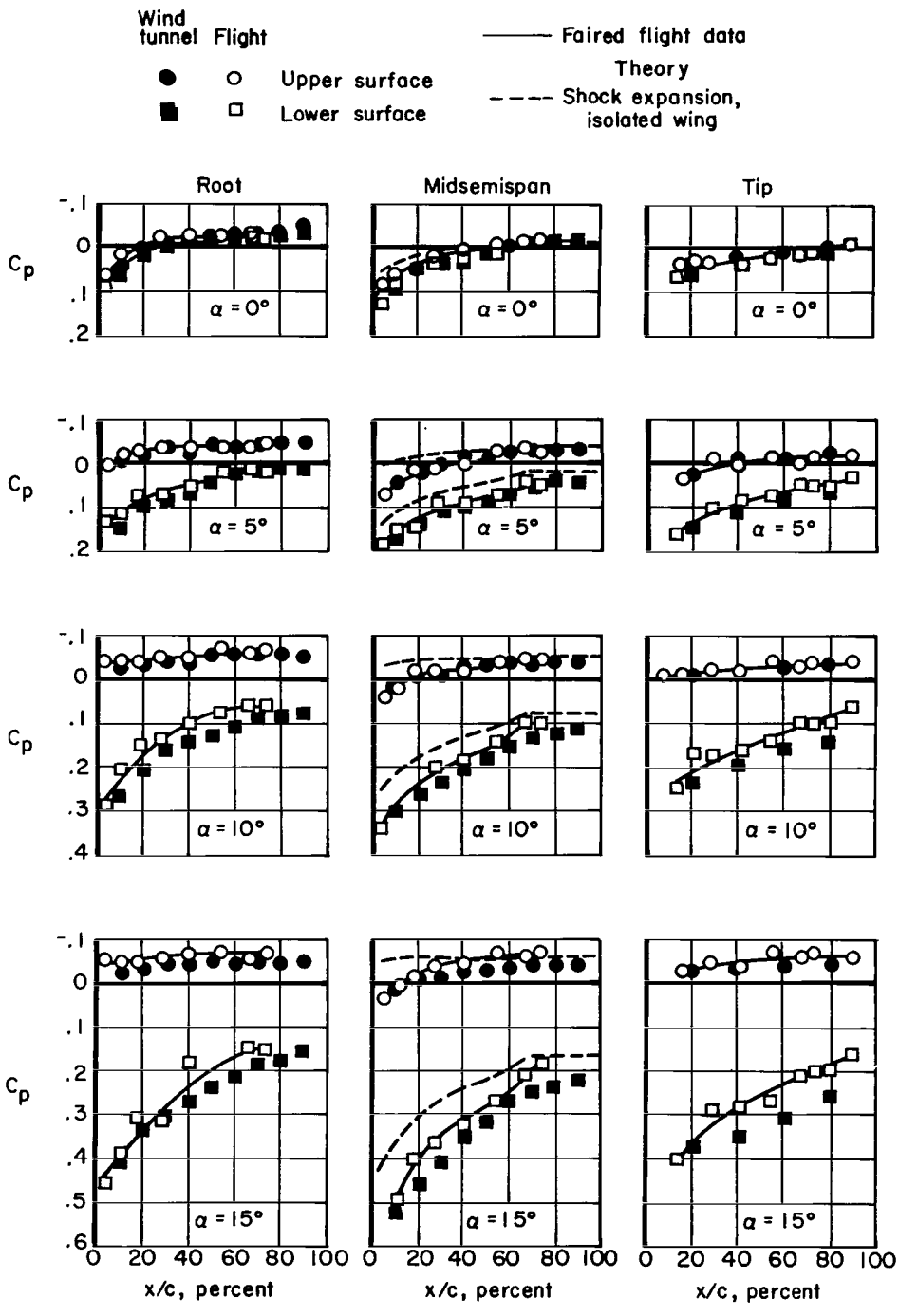

(g) M = 4.7.

Figure 4.- Continued.

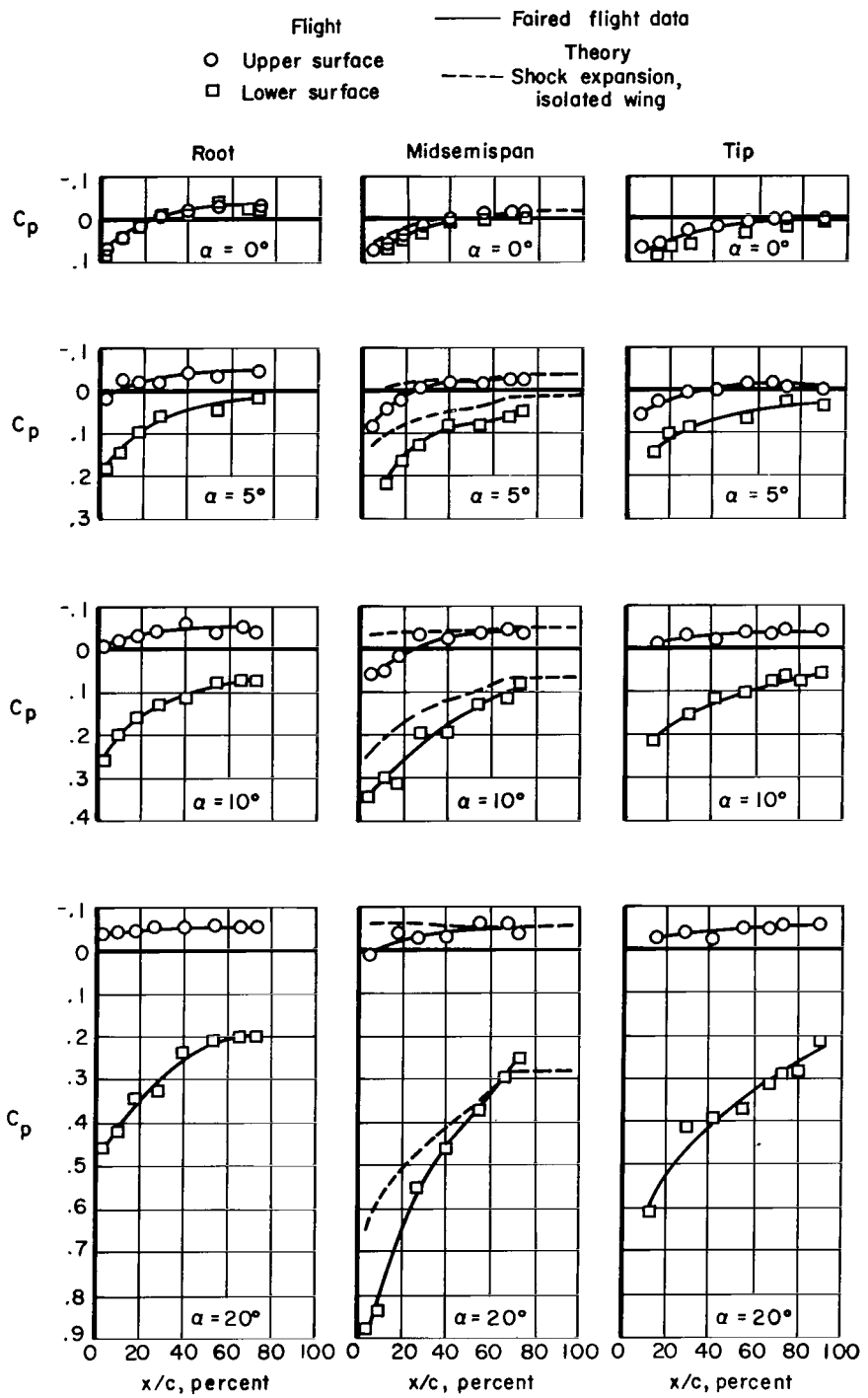

(h) M = 5.0.

Figure 4.- Continued.

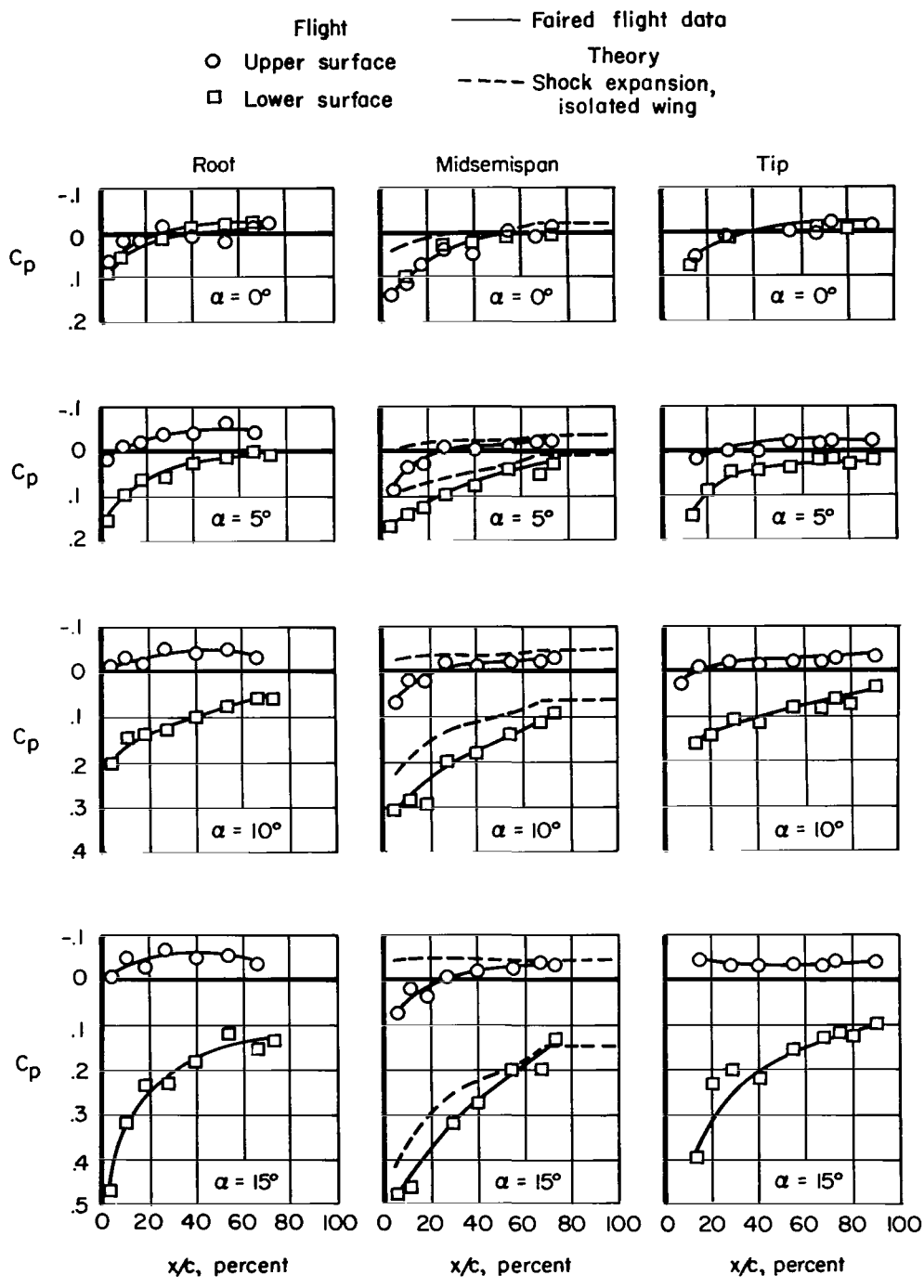

(i) M = 5.5.

Figure 4.- Continued.

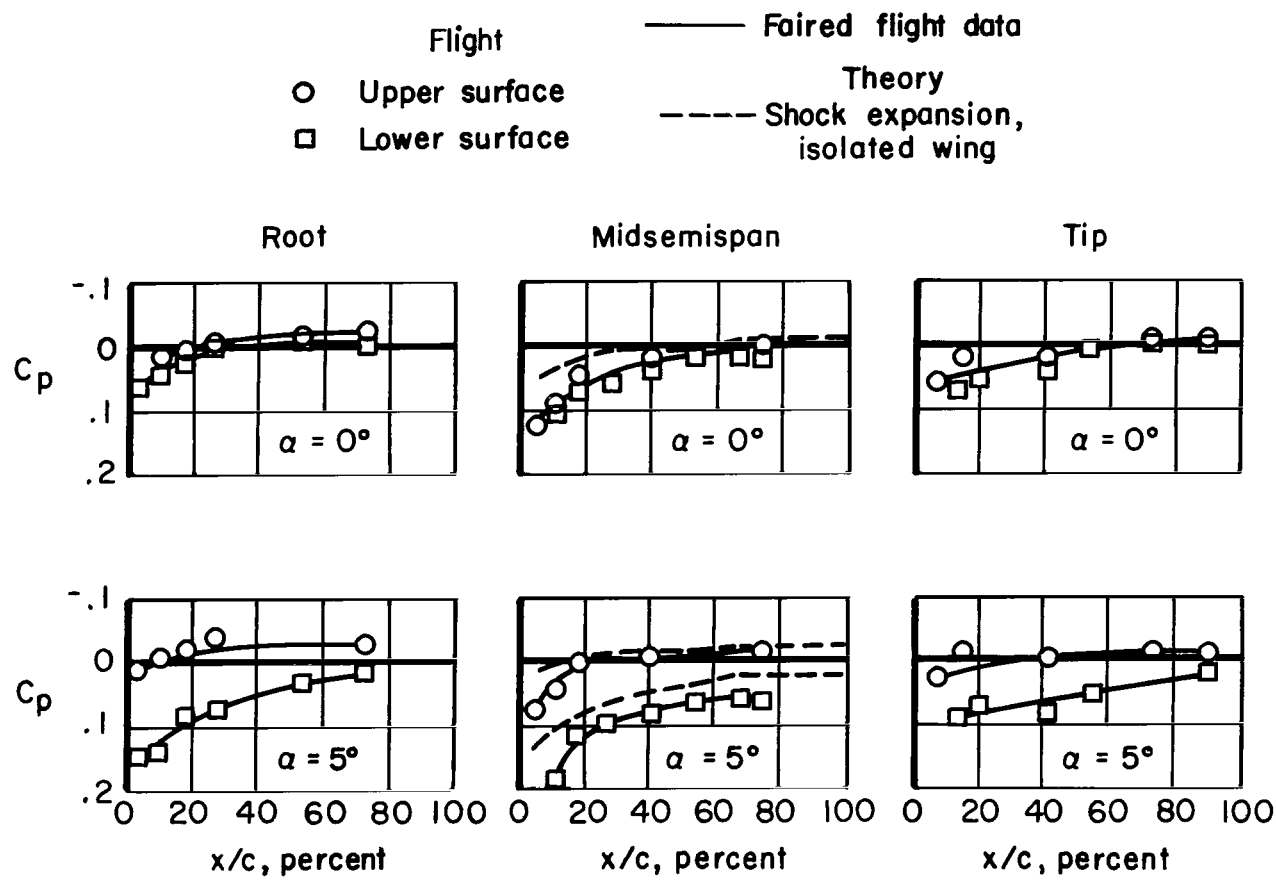

(j) M = 6.0.

Figure 4.- Concluded.

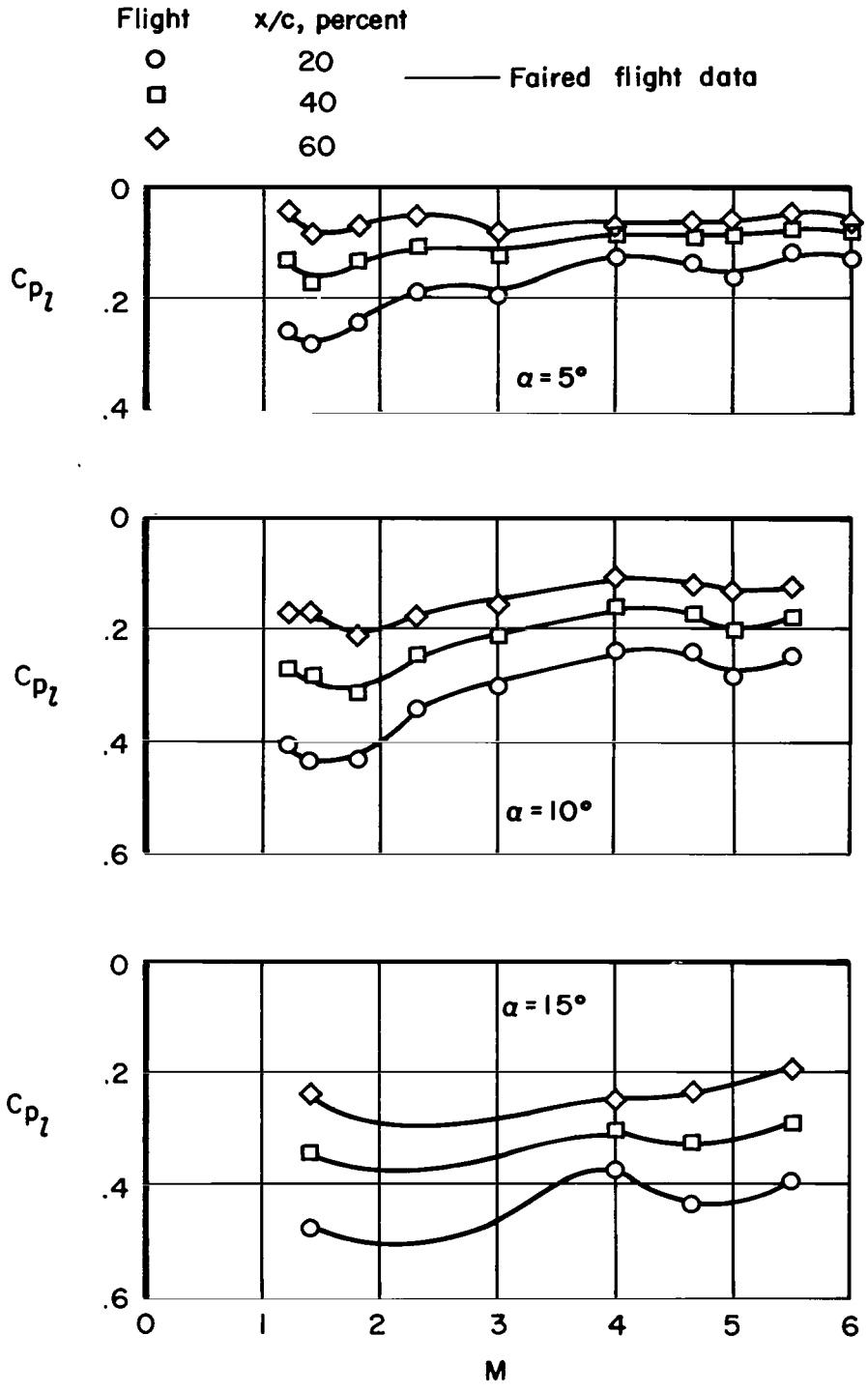

Figure 5.- Variation of midsemispan chordwise pressure distributions with Mach number on the lower surface of the X-15 wing.

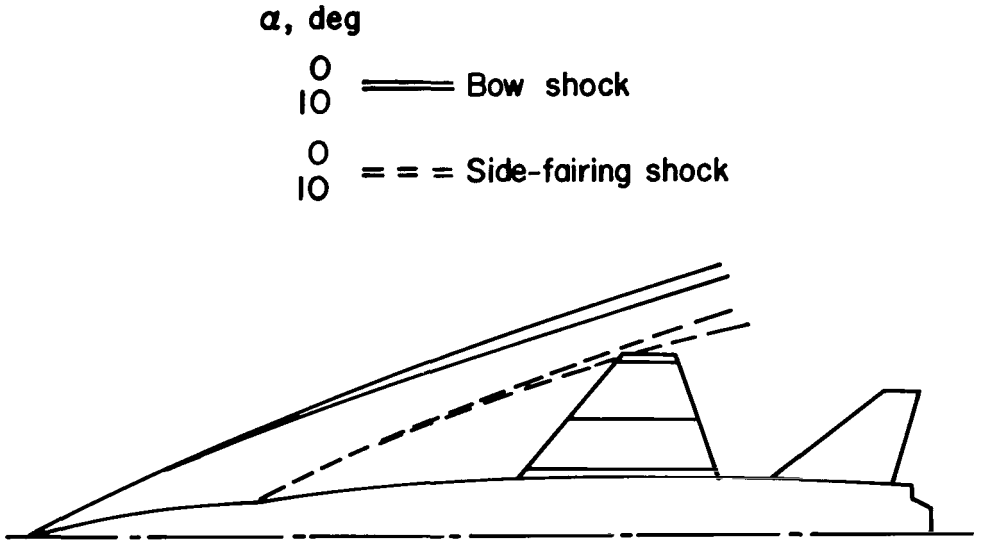

(a) M = 2.88.

(b) M = 4.65.

(c) M = 6.9.

Figure 6.- Wind-tunnel shock profiles over the X-15 wing.

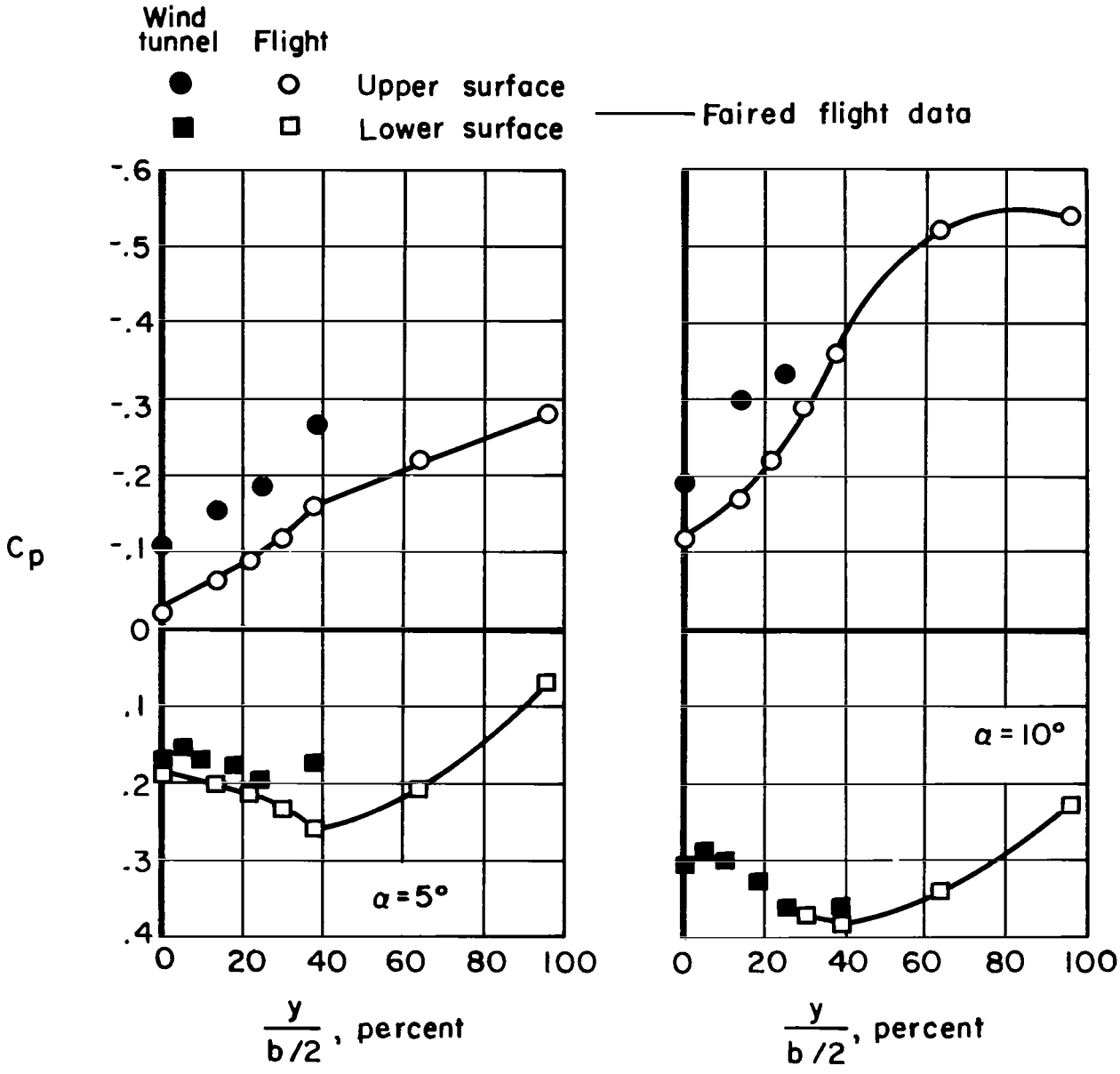

(a) M = 1.0.

Figure 7.- Wing-body spanwise pressure distributions.

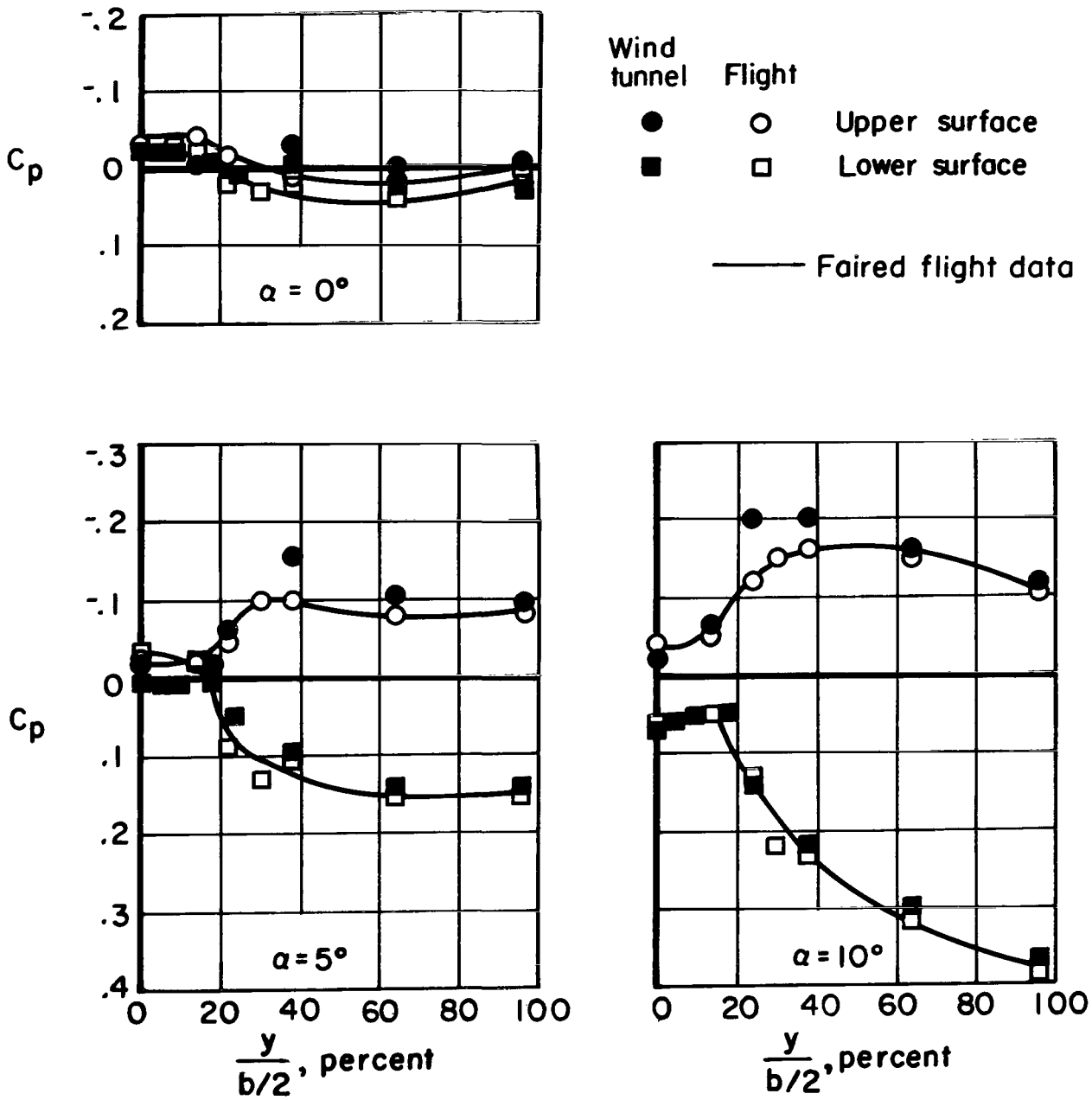

(b) M = 2.3.

Figure 7.- Continued.

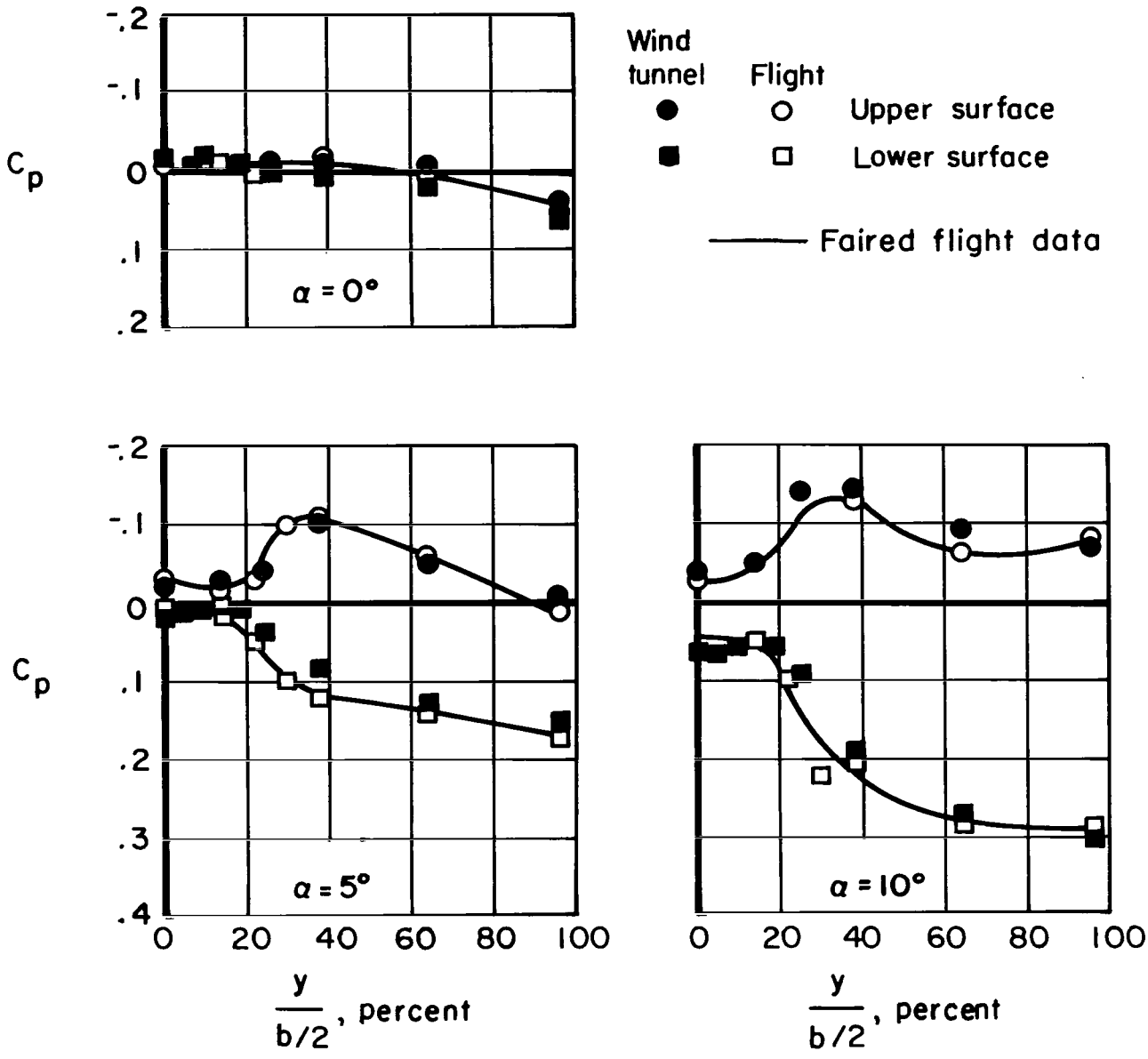

(c) M = 3.0.

Figure 7.- Continued.

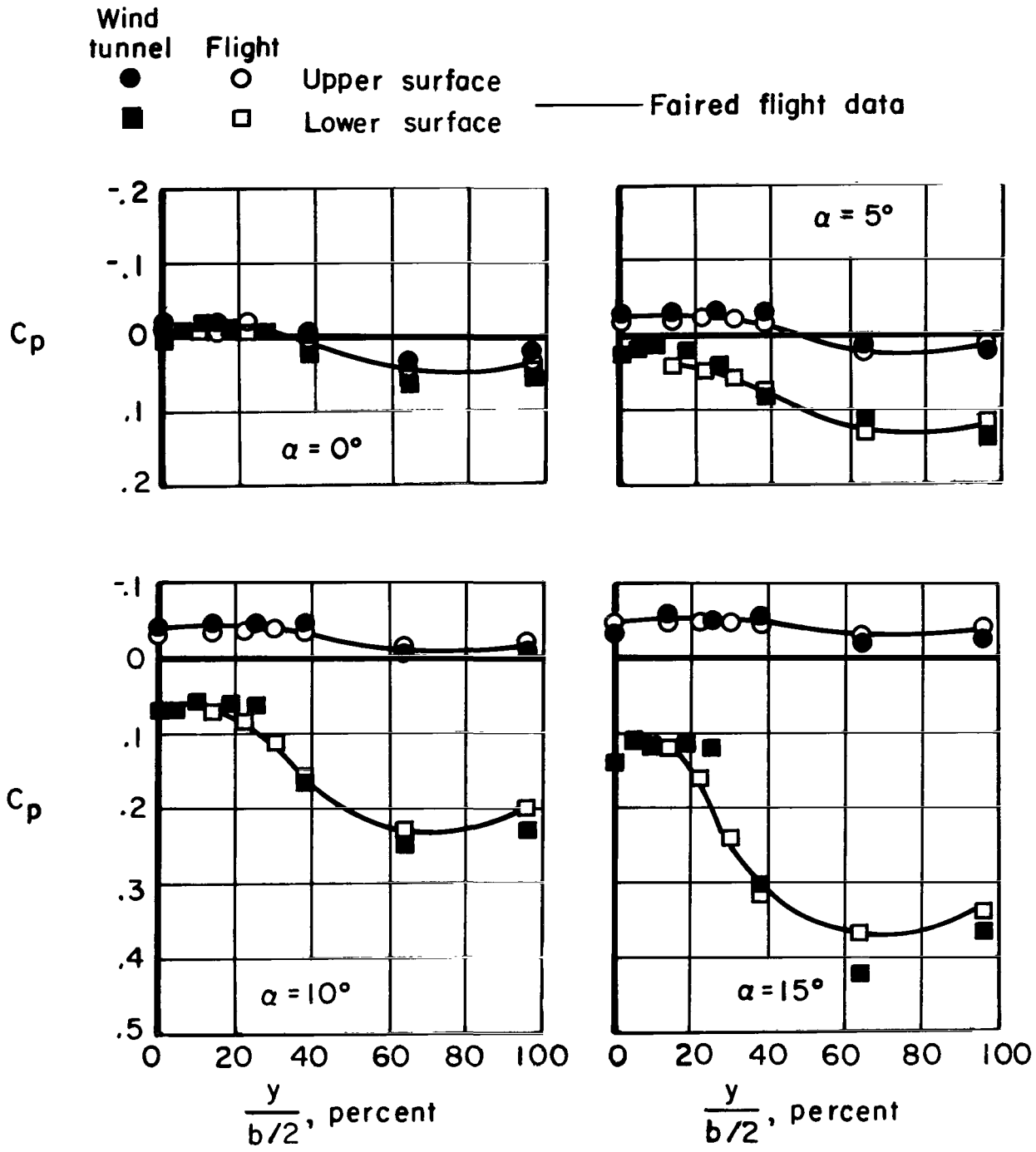

(d) M = 4.7.

Figure 7.- Concluded.

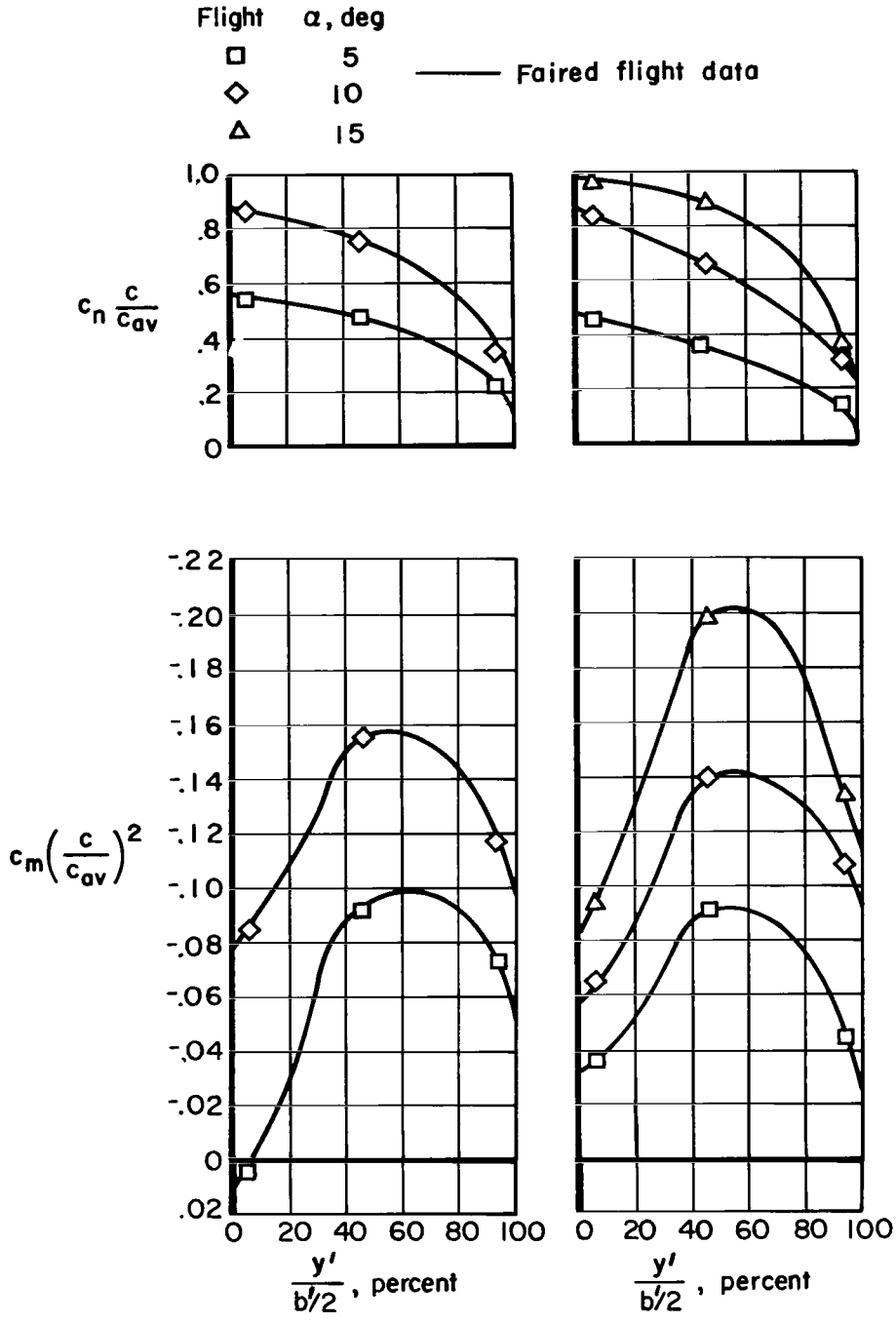

(a) M = 1.2. (b) M = 1.4.

Figure 8.- Wing section normal-force and pitching-moment coefficients at various angles of attack and Mach numbers.

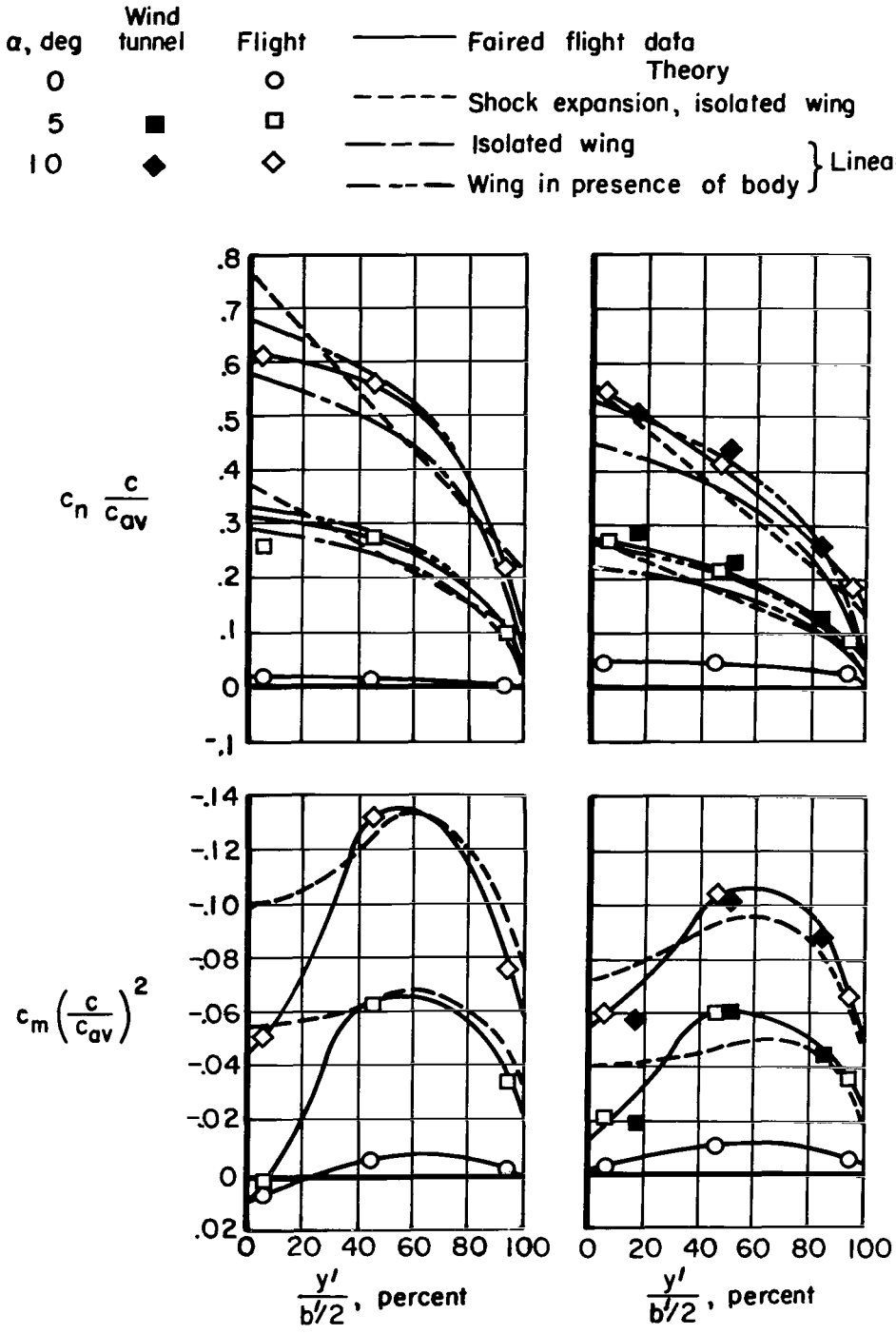

(c) M = 1.8. (d) M = 2.3.

Figure 8.- Continued.

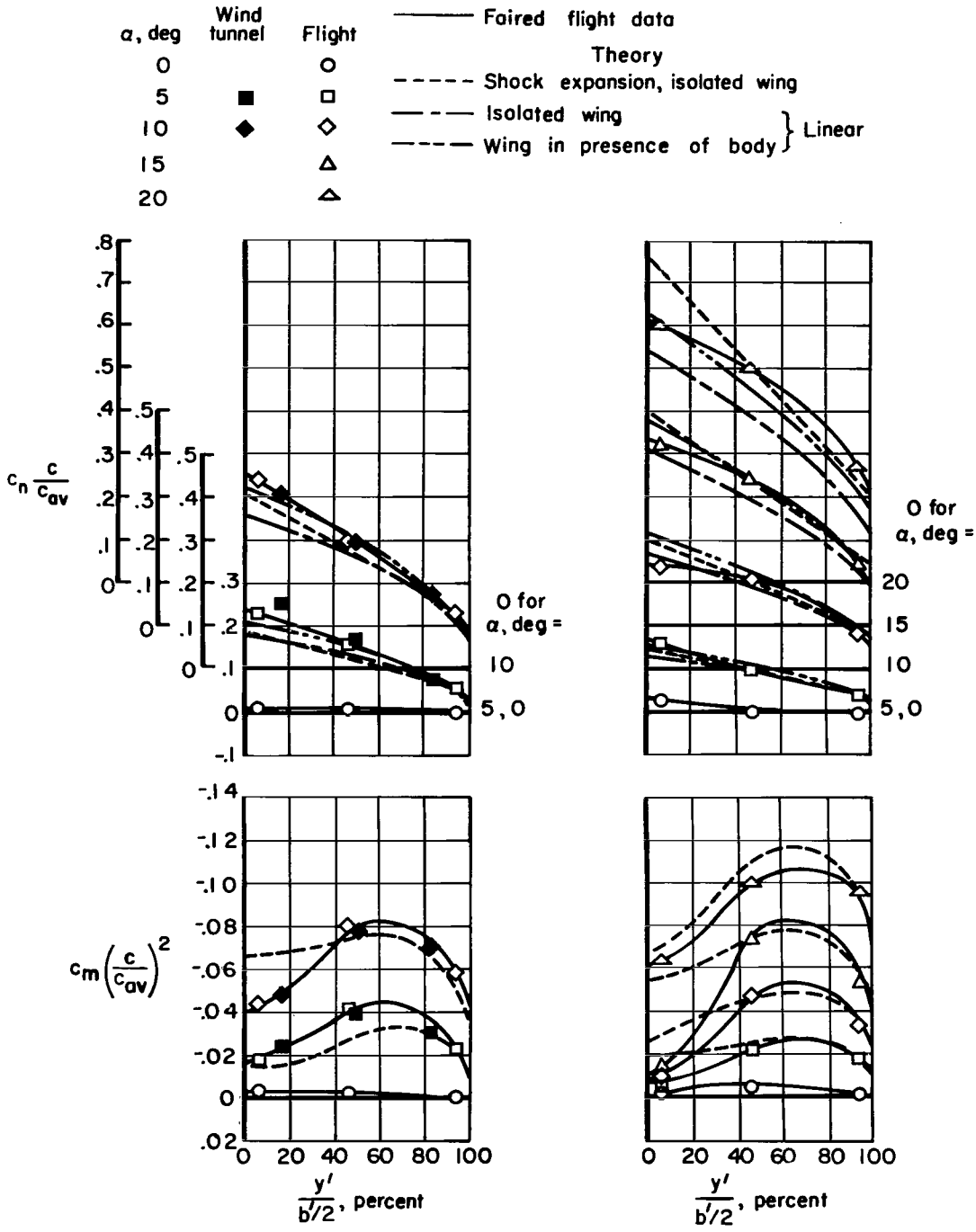

(e) M = 3.0. (f) M = 4.0.

Figure 8.- Continued.

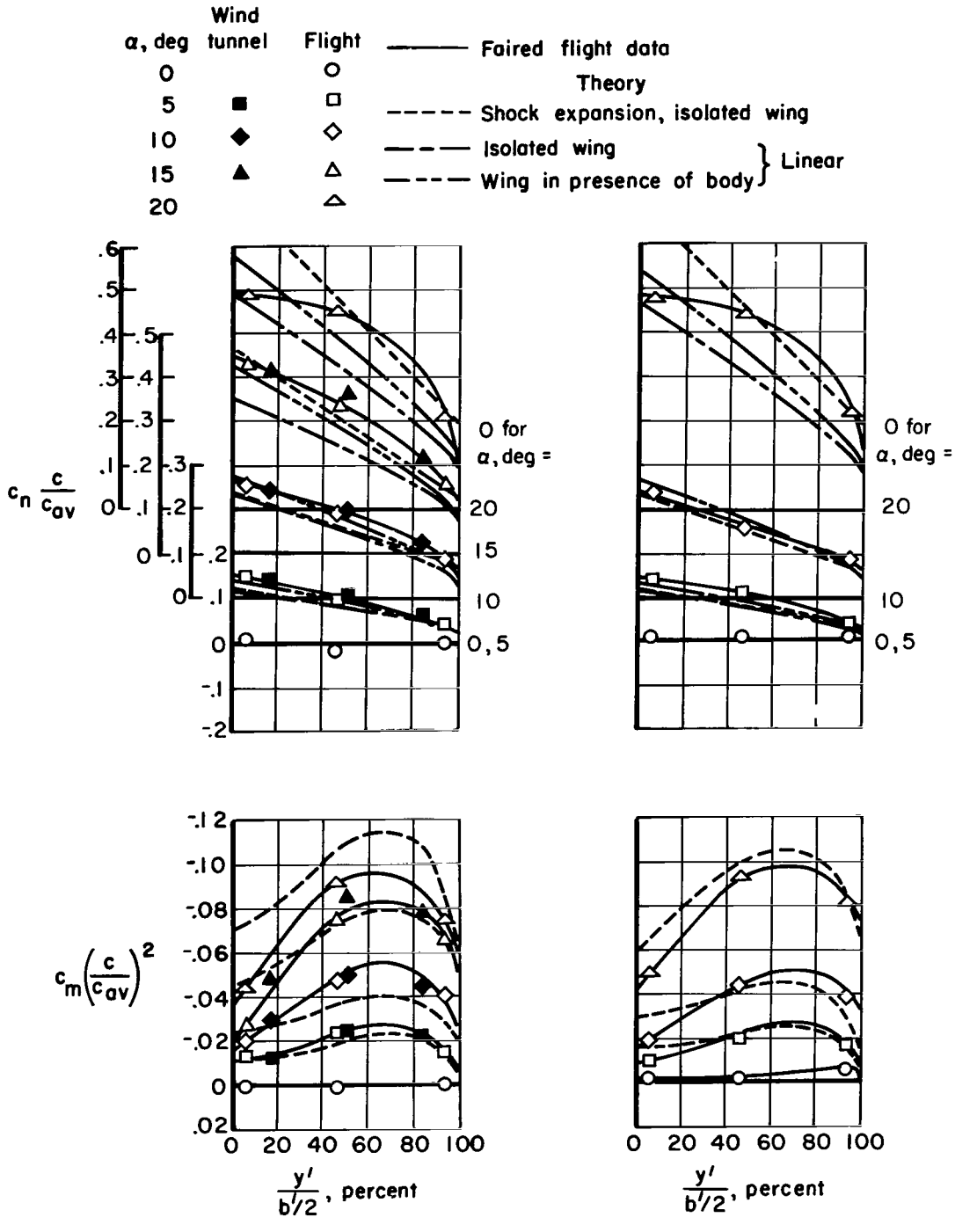

(g) M = 4.7.

(h) M = 5.0.

Figure 8.- Continued.

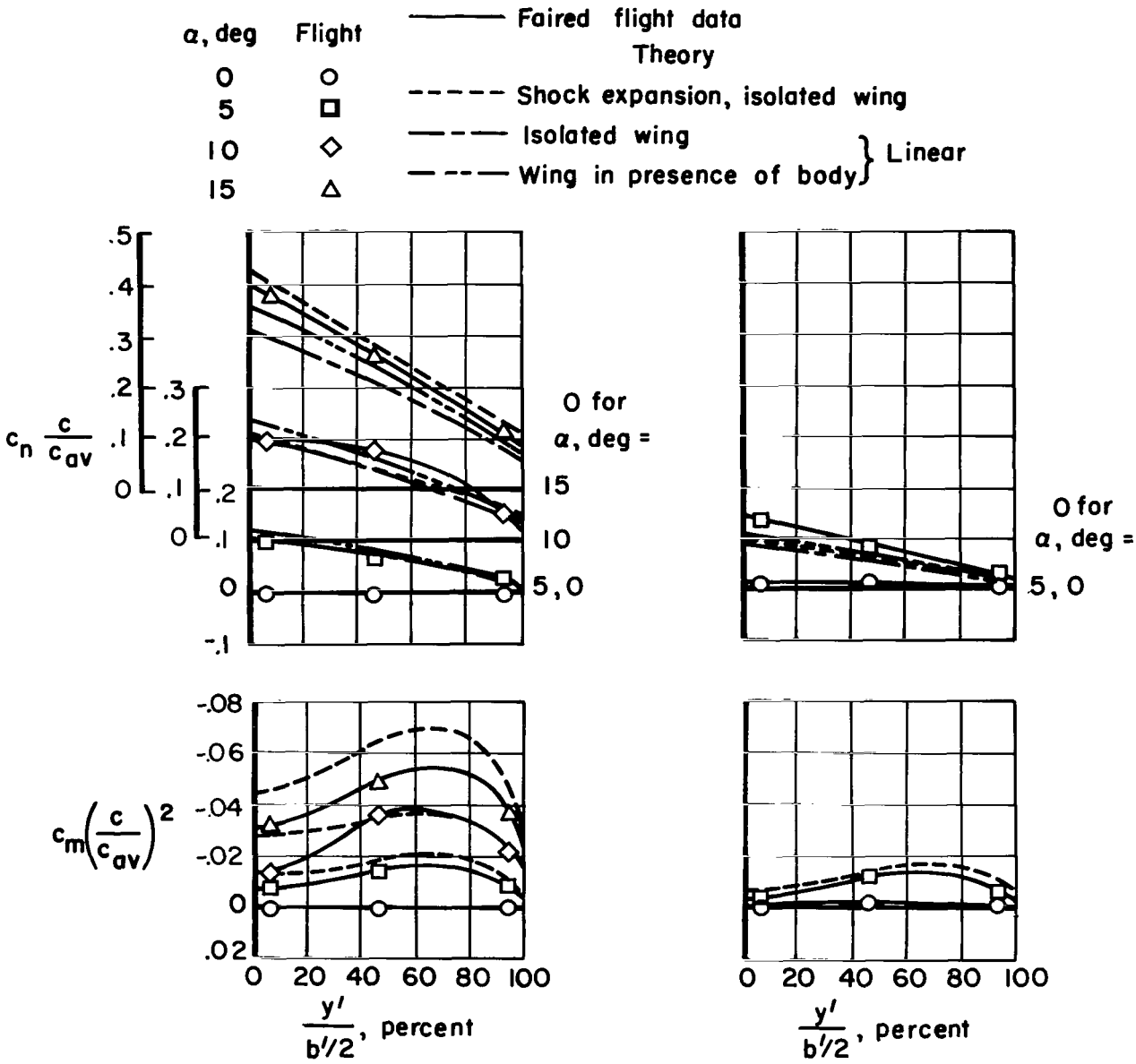

(i) M = 5.5.

(j) M = 6.0.

Figure 8.- Concluded.

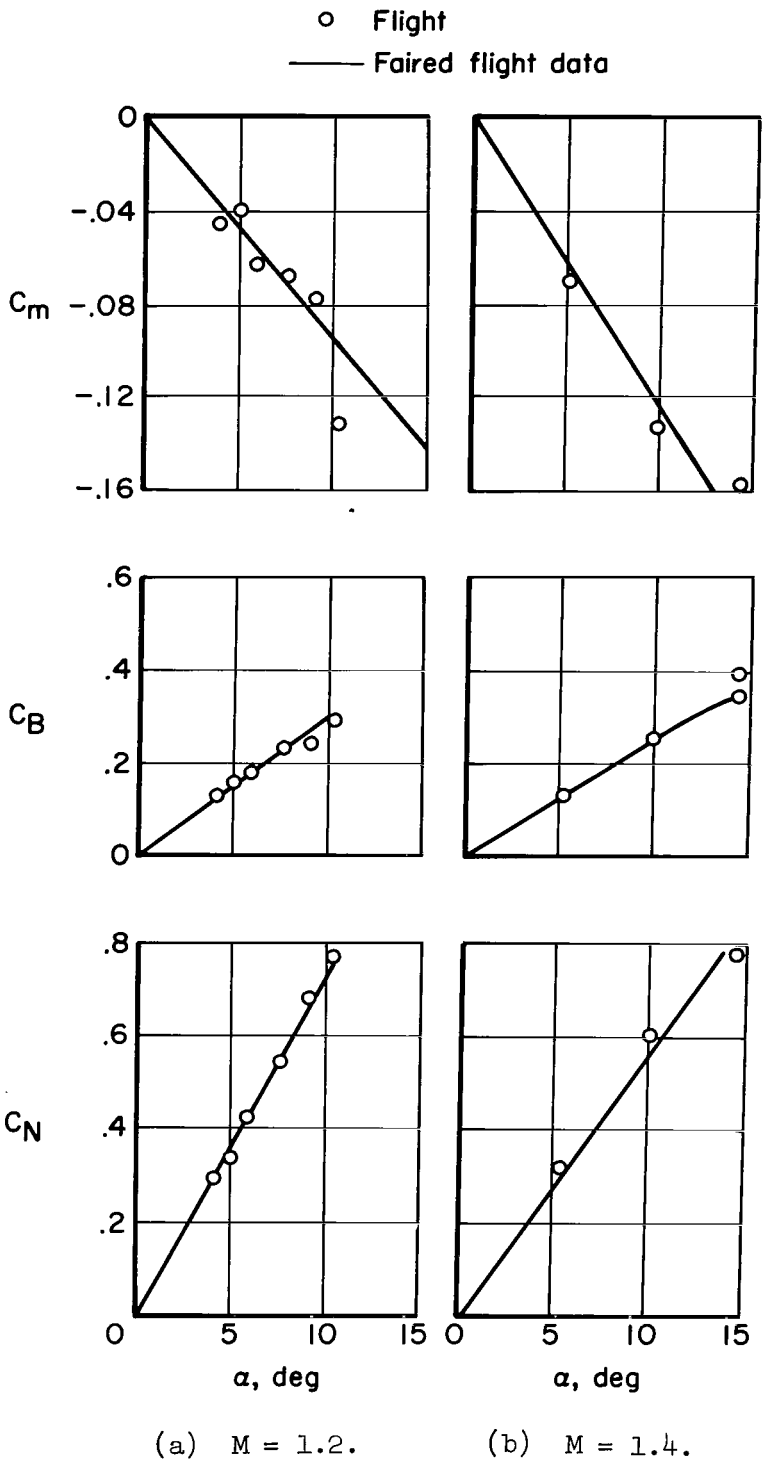

(a) M = 1.2. (b) M = 1.4.

Figure 9.- Comparison of wing load coefficients at various Mach numbers for the X-15 wing.

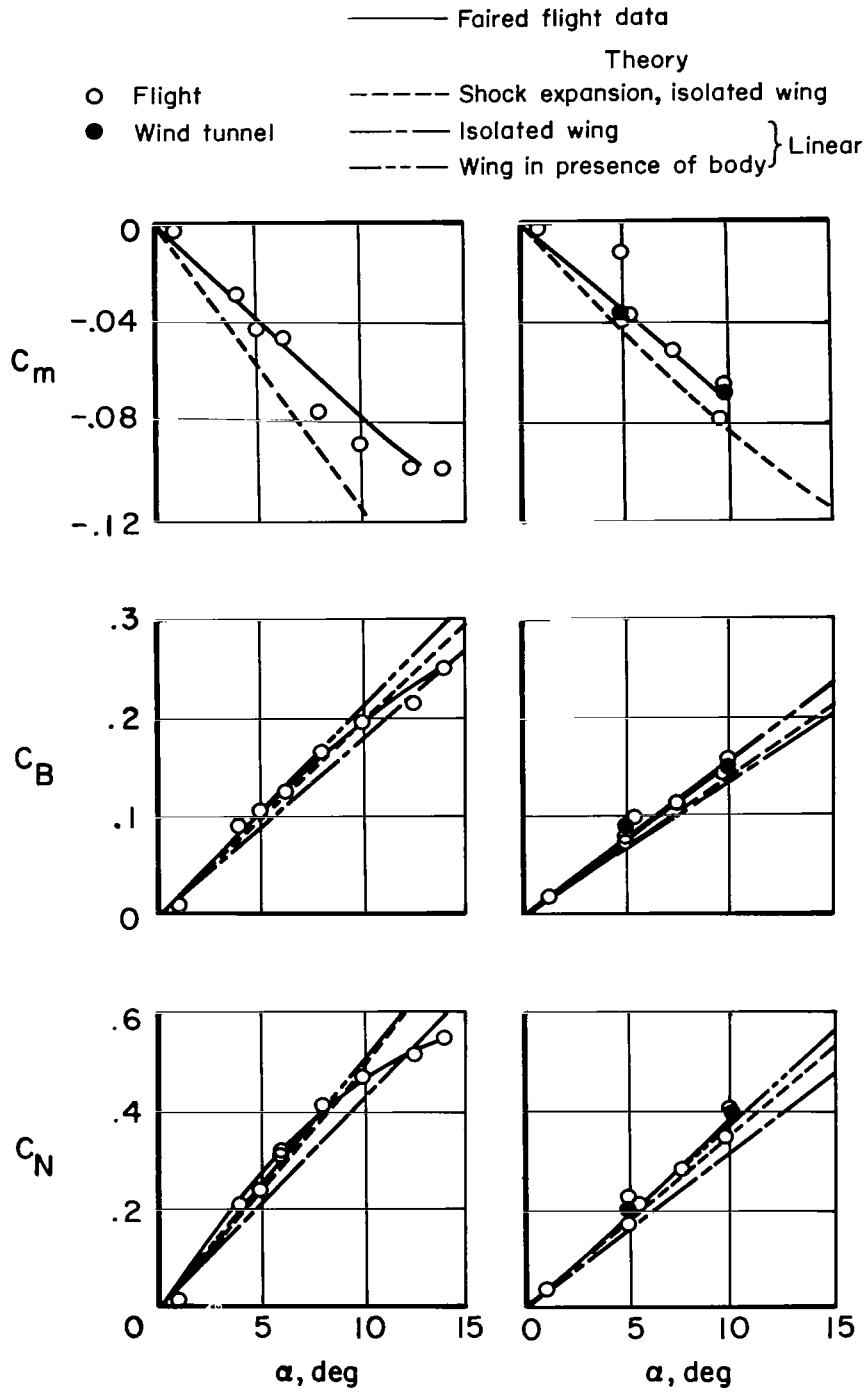

(c) M = 1.8. (d) M = 2.3.

Figure 9.- Continued.

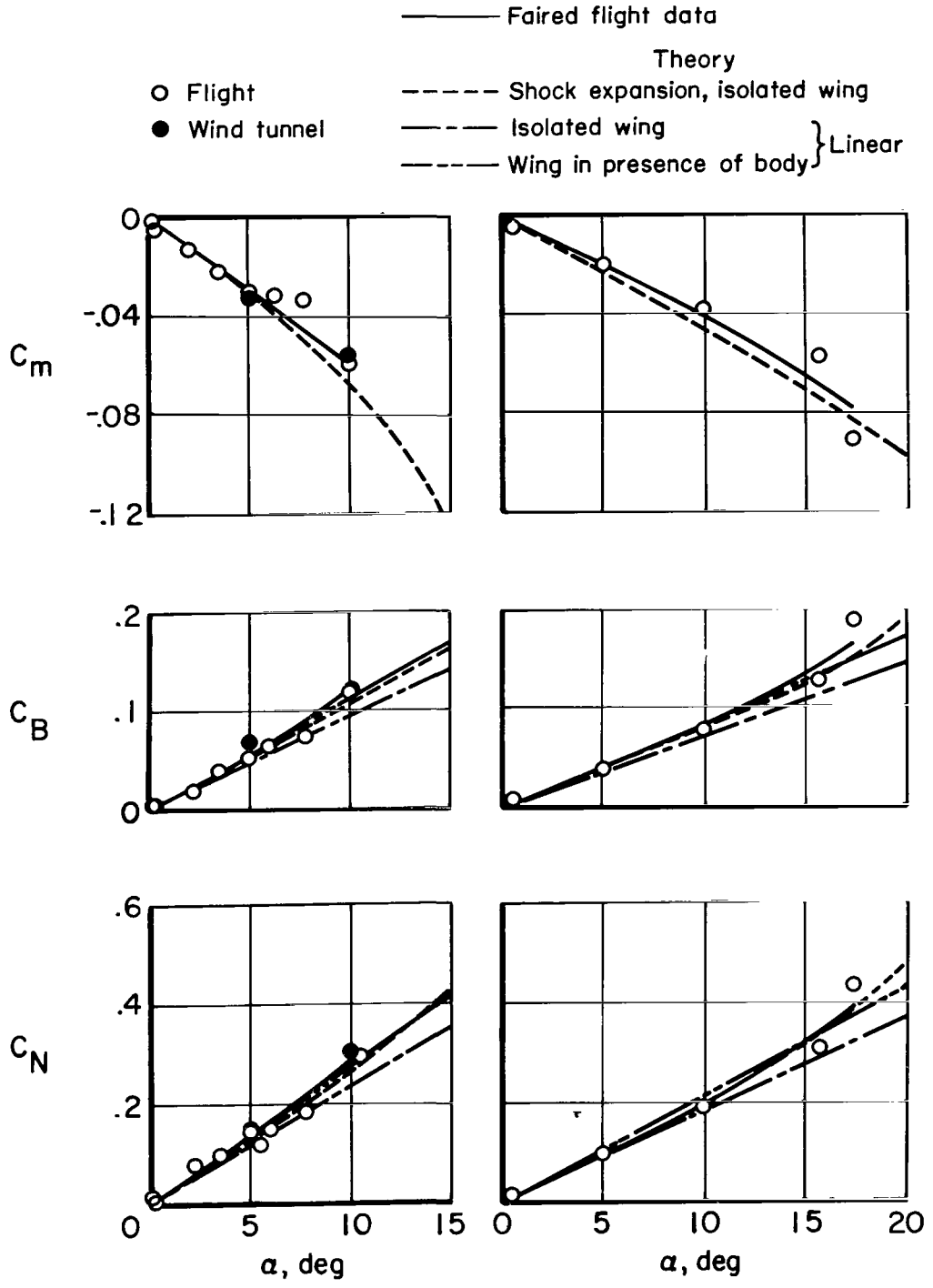

(e) M = 3.0. (f) M = 4.0.

Figure 9.- Continued.

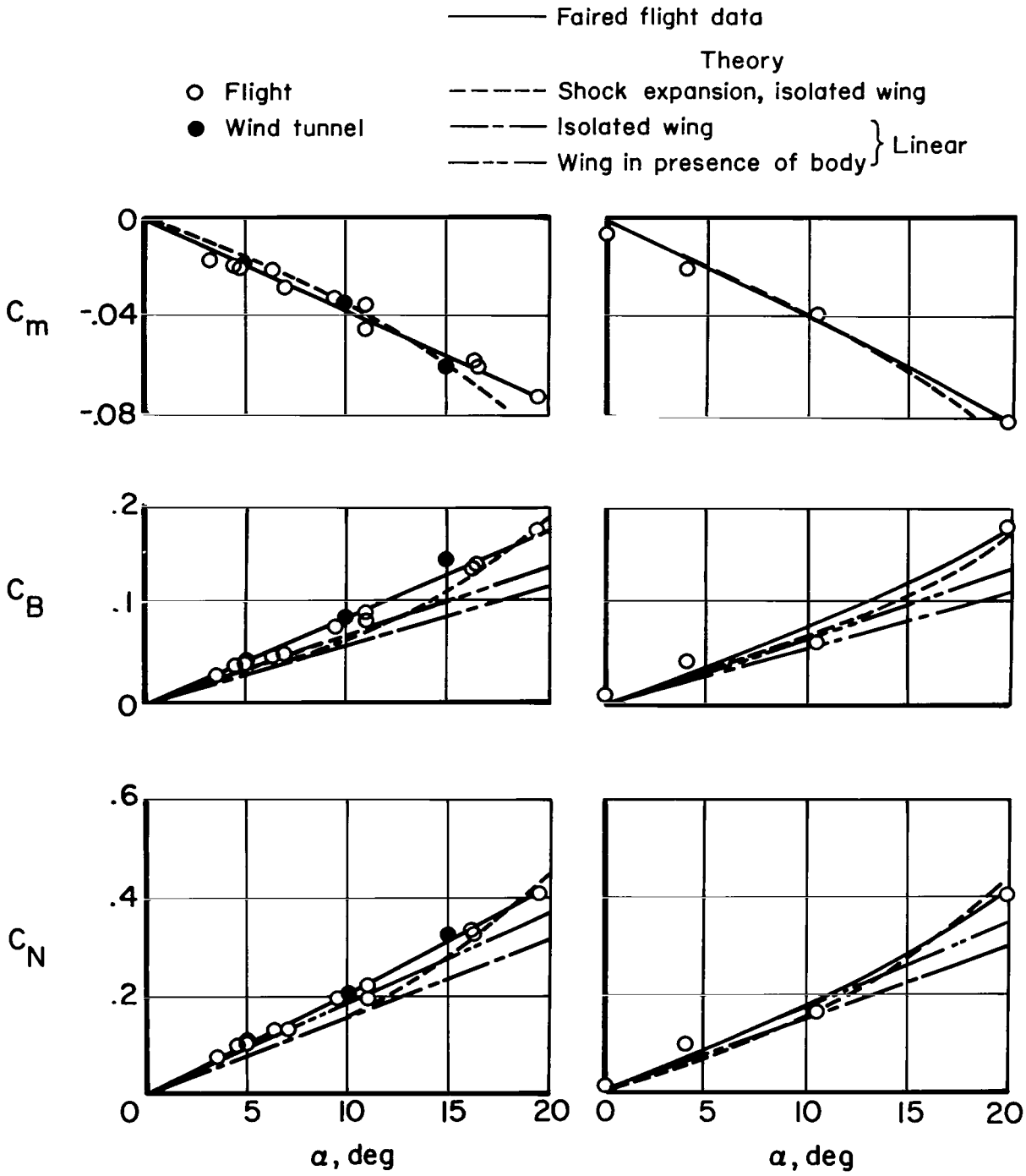

(g) M = 4.7.

(h) M = 5.0.

Figure 9.- Continued.

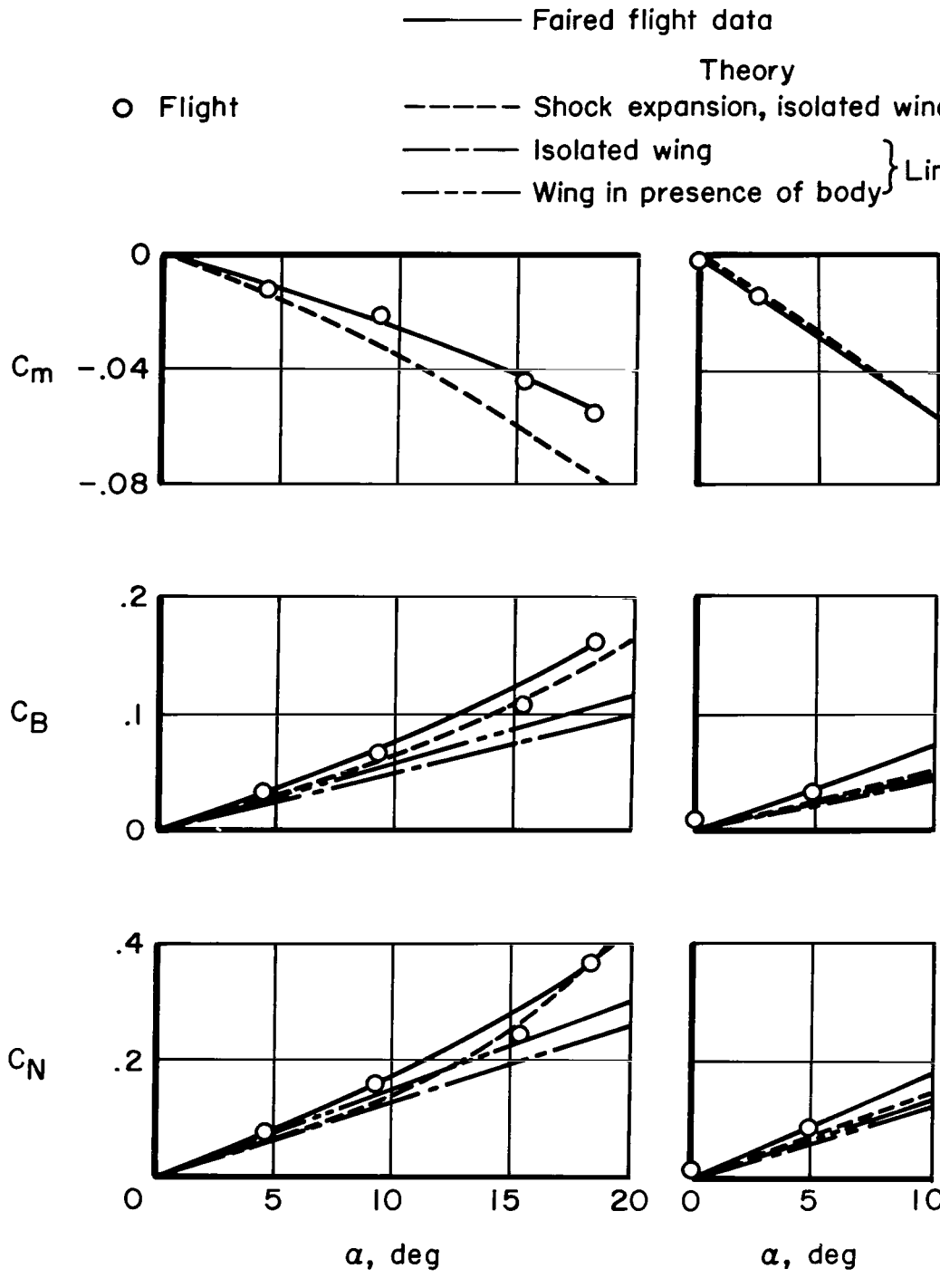

(i) M = 5.5. (j) M = 6.0.

Figure 9.- Concluded.

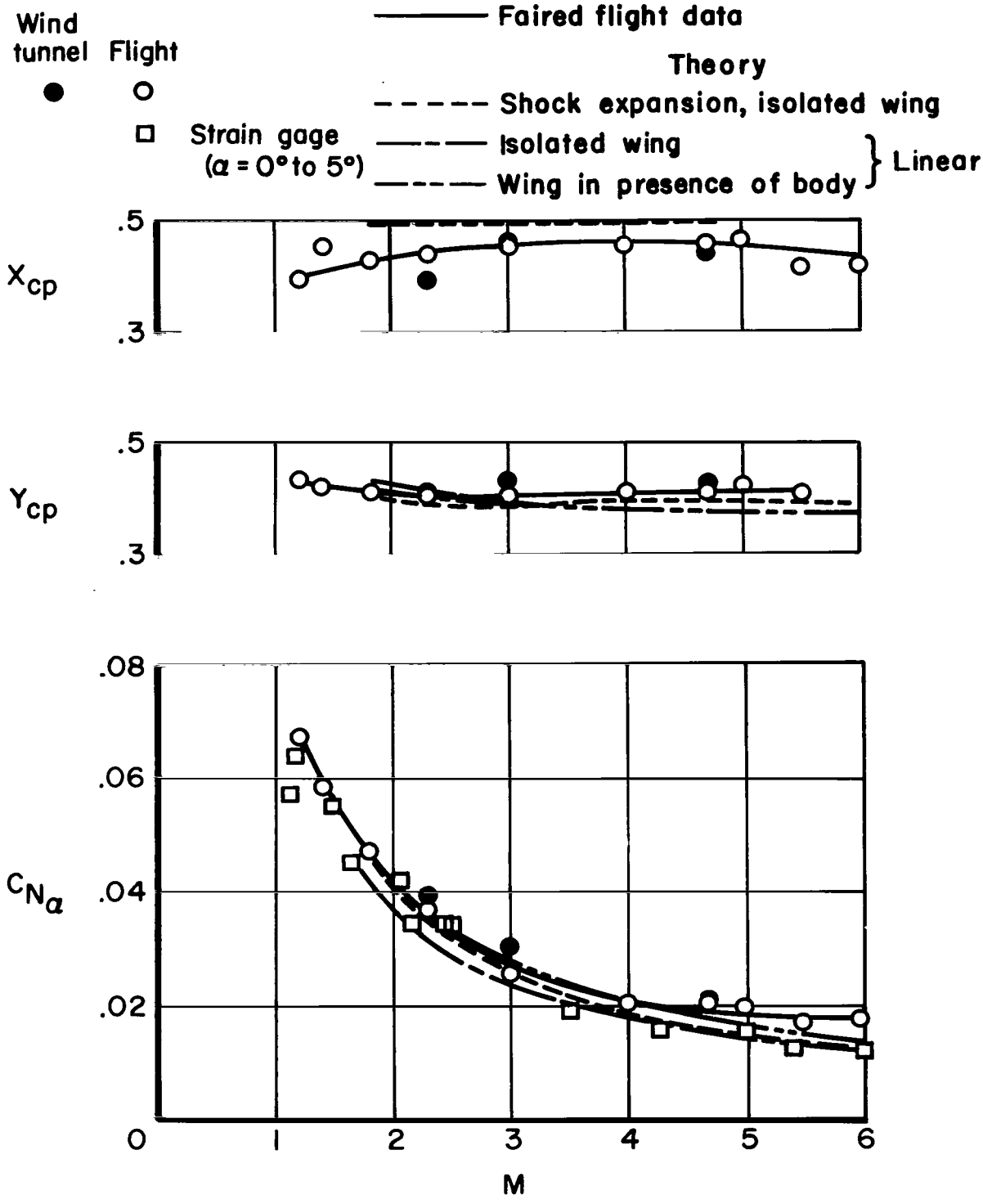

Figure 10.- Summary of aerodynamic loads on exposed wing of X-15.

"The aeronautical and space activities of the United States shall be conducted so as to contribute . . . to the expansion of human knowledge of phenomena in the atmosphere and space. The Administration shall provide for the widest practicable and appropriate dissemination of information concerning its activities and the results thereof."

—NATIONAL AERONAUTICS AND SPACE ACT OF 1958

NASA SCIENTIFIC AND TECHNICAL PUBLICATIONS

TECHNICAL REPORTS: Scientific and technical information considered important, complete, and a lasting contribution to existing knowledge.

TECHNICAL NOTES: Information less broad in scope but nevertheless of importance as a contribution to existing knowledge.

TECHNICAL MEMORANDUMS: Information receiving limited distribution because of preliminary data, security classification, or other reasons.

CONTRACTOR REPORTS: Technical information generated in connection with a NASA contract or grant and released under NASA auspices.

TECHNICAL TRANSLATIONS: Information published in a foreign language considered to merit NASA distribution in English.

TECHNICAL REPRINTS: Information derived from NASA activities and initially published in the form of journal articles.

SPECIAL PUBLICATIONS: Information derived from or of value to NASA activities but not necessarily reporting the results of individual NASA-programmed scientific efforts. Publications include conference proceedings, monographs, data compilations, handbooks, sourcebooks, and special bibliographies.

Details on the availability of these publications may be obtained from:

SCIENTIFIC AND TECHNICAL INFORMATION DIVISION

NATIONAL AERONAUTICS AND SPACE ADMINISTRATION

Washington, D.C. 20546